Energy Conversion and Management 256 (2022) 115370

Contents lists available at ScienceDirect

Energy Conversion and Management

journal homepage: www.elsevier.com/locate/enconman

Optimal sizing of a hybrid PV-WT-battery storage system: Effects of split-ST and combined ST + ORC back-ups in circuit charging and load following

Godfrey T. Udeh [a,b], Stavros Michailos [b,*], Derek Ingham [b], Kevin J. Hughes [b], Lin Ma [b], Mohamed Pourkashanian [b]

[a] Department of Mechanical Engineering, Faculty of Engineering, University of Port Harcourt, Nigeria
[b] Energy 2050, Department of Mechanical Engineering, University of Sheffield, Sheffield S3 7RD, United Kingdom

ARTICLE INFO

Keywords:
Techno-enviro-economic
Multi-objective optimisation
Split ST back-up
Combined power
Dispatch strategy
TOPSIS

ABSTRACT

This study explores the opportunities in deploying split Stirling and combined Stirling and organic Rankine cycle (ORC) in circuit charging and load following dispatch modes, respectively as the back-up of a hybrid renewable energy system. The optimal number of system components in each dispatch mode that simultaneously minimises the loss of power supply probability (LPSP), levelised cost of energy (LCOE) and dumped power have been found by implementing an evolutionary algorithm-based multi-objective optimisation approach. Then, a multi-criteria decision making tool is deployed to select the best configuration from the Pareto set. The optimal hybrid system configuration obtained have been compared to the traditional diesel generator back-up system base case, to demonstrate performance improvements with the deployment of the proposed back-ups. The results show deploying Stirling + ORC back-up in load following leads to 60.70% and 33.71% reductions in the LCOE and CO_2 emissions, respectively compared to the base case but with slightly higher LPSP. While 61.4%, 33% and 24.47% reductions in the LCOE, CO_2 emissions and LPSP have been observed with the deployment of split Stirling in circuit charging mode. Further results from the dynamic simulation highlight the energy cost, reliability, dumped power and battery performance of the optimal system respond to seasonal changes in the test location. Other observed results show the change in the market price and number of the photo-voltaic generator that generates 50% of the total power, strongly affect the performance of the optimal system. The proposed biomass powered Stirling based back-ups are promising alternatives to replace the traditional diesel generator back-ups in improving the green energy system's reliability.

1. Introduction

Green energy solutions hybridising many renewable energy resources are becoming more competitive for meeting the energy demand at off-grid locations, mainly because of the steady decline in the cost of system components and improving efficiencies. Most renewable energy resources, especially solar and wind, are spasmodic in nature; hence, it is compelling to hybridise them so as to improve their reliability and minimise costs [1]. Notwithstanding the improved reliability of hybrid renewable energy systems (HRES), back-up power blocks are still required to minimise the mismatch between the electricity generation from these stochastic resources and the demand [2–3]. Internal combustion (IC) engines, such as the diesel generator (DG) have been popularly deployed as the back-up in HRES, and are in some designs combined with battery storage. There are also HRES configurations that deployed external combustion engines, such as the Stirling engine (ST), organic Rankine cycle (ORC) and micro-turbine (MT) or even fuel cell (FC), as the back-up.

Hybrid renewable energy systems present different unique configurations depending on the available local resources [4]. This also suggests that they may contain many components, and would require some complex control strategies to coordinate their operation. Consequently, it is necessary to optimally determine the best HRES configuration considering the available local resources, the weather data, the control strategies and the load characteristics of the intended users. Due to the complexity, non-convex nature and non-linearity of the mathematical models used to predict the performance of HRES components, and the many plausible combinations of components and strategies, memetic algorithms have been popularly deployed to determine the optimal number of the system components [5–6]. Also, the sizing of HRES has

* Corresponding author.
E-mail address: s.michailos@sheffield.ac.uk (S. Michailos).

https://doi.org/10.1016/j.enconman.2022.115370
Received 23 October 2021; Received in revised form 8 February 2022; Accepted 9 February 2022
Available online 16 February 2022

been performed in the literature using single and multi-objective optimisation approaches that are formulated based on technical, economic, environmental and social considerations.

Several recent studies on sizing optimisation of different HRES configurations have been undertaken from single and multi-objective perspectives. Kraa et al. [7] obtained the optimum number of wind turbines (WT), solar photovoltaic panels (PV) and battery storage systems (BSS) required in a HRES system, by minimising the 20-year round total system cost. Dufo-Lopez and Cristobal-Monreal [8] found the optimal configuration of a HRES, by solely minimising the weight or the cost of energy (COE) of the system as the objective function. Ramli et al. [9] sized the components of a hybrid WT, PV, BSS, with DG back-up system designed to supply the electric load of a location in Saudi Arabia. They found the optimal system configuration by simultaneously minimising the loss of power supply probability (LPSP), renewable fraction (RF) and COE. It was reported that a decrease in the number of PV in the optimal configuration leads to an increase in the LPSP, i.e., high reliance of the system on the DG back-up. Wu et al. [10] found the optimal system configuration by minimising the total system cost and power curtailment of a WT, PV, battery and MT back-up HRES and observed some reductions in power curtailment cost with the deployment of battery storage. Barakat et al. [11] determined the optimal number of components of a WT, PV, BSS and DG back-up system for a location in Egypt, by considering the LPSP, COE and RF as the objective functions.

Yuan and Zhao [12] studied the optimal sizing of a standalone solar, wind, battery and DG back-up system designed for Dongao island, China, by minimising the annual total cost and pollutant emissions, using a novel improved fruit fly optimisation algorithm. They revealed that the configuration without DG back-up produced zero emissions; however, it was comparatively too expensive. This result further highlights the conflict between emissions and the cost of energy. Moradi et al. [13] optimally sized the components of a HRES system that contains WT, PV and deploys DG, MT and FC as back-ups, while excess power produced is stored in ultra-capacitors and BSS. The authors minimised the cost and emissions of the system and reported 8.5% savings in cost when BSS is deployed to store the excess power. Rathish et al. [14] considered the number and types of the components as the decision variables in the multi-objective sizing of a hybrid WT and PV system with DG back-up. Also, they adopted the net present cost (NPC), unmet load and CO_2 emissions as the objective functions and found the optimal system using a genetic algorithm (GA) based multi-objective evolutionary algorithm (MOEA). Dufo-Lopez et al. [15] performed sizing optimisation of a solar PV, WT and DG back-up HRES, based on the simultaneous minimisation of cost and maximisation of the human development index (HDI) and job creation (JC).

Sadeghi et al. [16] demonstrated that the introduction of electric vehicles (EV) into a hybrid WT, PV and BSS system improves the reliability of the system, by comparing the LPSP of the HRES with and without EVs. First, the authors found the optimal number of components of the HRES through the simultaneous minimisation of the life cycle cost (LCC) and LPSP, before simulating its dynamic behaviour with the introduction of EVs. Xu et al. [17] found the optimal size of the components of a standalone PV, WT, hydro-power system by considering two objectives: the levelised cost of energy (LCOE) and LPSP. It was observed that a decrease in the curtailment ratio of the wind turbine power leads to an increase in the LCOE and they recommended reducing the size of the WT and PV to minimise the dumped power. Bukar et al. [18] minimised the COE and deficiency of power supply probability (DPSP) by deploying the grasshopper optimisation algorithm (GOA), to obtain the optimal size of the components of a HRES comprising solar, wind, battery and DG back-up. This study increased the penetration of renewable resources in the system, by constraining it to a DPSP of 0% and realised high dumped power and COE of 0.36 $/kWh, due to the oversizing of the WT and PV generators.

It is clear from the presented literature that power curtailment and the use of fossil fuel powered back-ups are some of the main issues affecting the cost, emissions and reliability of HRES. Nonetheless, the deployment of split DG appears to be promising to minimise the emissions, dumped power and cost of HRES with DG back-up. Ayodele et al. [19] found the optimal number of system components of a hybrid PV, WT, battery system with three-split DG back-up, by minimising the LCC, CO_2 emissions and dumped power. The authors regulated the hourly commitment of the DGs to the HRES, by operating at any time, a minimum number of DGs to match the deficit power in the system. They compared the results to single DG back-up system and found 46%, 28%, 82%, and 94% reductions in LCC, COE, CO_2 emissions and dumped power, respectively.

Other studies have deployed biomass fired engines or fuel cells as back-ups to reduce the emissions and the cost of energy of HRES. Gonzalez et al. [20] found the size of the components of a solar, wind and biomass grid connected energy system by optimising the LCC and life cycle environmental impacts using GA. It has been reported that the optimum HRES has low environmental impact and cost compared with the DG back-up system. Sawle et al. [21] sized a HRES comprising WT, PV and biomass back-up power and compared the results from two different optimisation approaches. Maleki et al. [22] performed the cost optimisation of a grid integrated HRES comprising solar PV, WT, solar thermal collector and FC and found the optimal system configuration. Ghaem Sigharchian et al. [23] investigated the feasibility of deploying biogas driven gas engine as a back-up for a solar PV-WT system designed for Garissa community in Kenya. Patel and Singal [24] proposed a generator fired by biofuel from wheat straw, mustard stalks and fuel wood, and biogas from animal dungs as the back-up in a WT-PV HRES, designed for a village settlement in India.

Although biomass driven back-up has been deployed by a few studies to augment the power supply of HRES, there are limited studies that proposed ST as the back-up in HRES configurations. Stirling engines have many attractive features: good part load performance, quiet operation, low vibration, easy maintenance and ability to utilise multiple clean energy sources of low, medium and high grade quality, such as biomass fuels [25–26]. The limited deployment of ST to augment the reliability of HRES may be as a result of its low electrical efficiency especially at micro-power scale [27–28]. Even so, this challenge can be overcome by exploring combined cycle configurations. Also, the high emissions and cost of energy that characterize the deployment of DG back-up, particularly when it is compelled to operate outside the rated conditions whilst following the load could be minimised by a similar approach. It is well established that combined power generation whereby the exhaust waste heat of the topping cycle is recovered by the bottoming cycle, results in improved efficiency, and reduces the consumption of primary energy and emissions. In particular, Udeh et al. [29] reported 63.4% increase in the electrical efficiency of a combined ST and ORC bottoming cycle powered by biomass.

To the best of our knowledge, there are limited recorded studies in the literature where a biomass fired ST + ORC has been deployed as the back-up in a HRES. Further, although there are evidence of studies deploying split DG to reduce the dumped power and emissions from a HRES, there are no records of studies where a renewable spilt solution, such as the split ST has been deployed in a HRES. Moreover, the issue of excessive power dumping, especially for standalone HRES can be mitigated at the design stage of the system, by including dumped power as one of the objective functions.

Overall, this paper therefore proposes the deployment of two new biomass powered back-ups to augment the reliability of a hybrid PV, WT and BSS energy system. The optimal number of system components that simultaneously minimises the levelised cost of energy, loss of power supply probability and dumped power will be found by deploying a memetic algorithm. The optimal system will be compared to the sole DG back-up base case and sole ST from the stand-points of reliability, cost, emissions and dumped power.

The main contributions of this study are summarised as follows:

Proposing a novel HRES configuration that deploys a carbon neutral biomass fired combined ST and ORC as the back-up and undertaking the system sizing optimisation by the simultaneous minimisation of the LCOE, LPSP and dumped power.

Investigating the impact of using 4-split ST instead of one big ST or DG as the HRES back-up in circuit charging mode on the reliability, cost, emissions and dumped power of the system.

Evaluating the reductions in the greenhouse gas emissions, dumped power, LCOE and LPSP of the HRES utilising combined ST + ORC back-up compared to sole ST or DG back-up in load following mode.

This paper has been structured as follows: Section 2 presents the configuration of the HRES. Section 3 formulates the mathematical models deployed in predicting the performance of the components of the HRES and develops the objective functions and constraints. In addition, the rule-based dispatch strategies for managing the energy system is presented in this section. Section 4 discusses the solution algorithm and the methodology for implementing the optimisation problem. This section also presents the multi-criteria decision making scheme deployed to select the optimum configuration from the Pareto optimal set. Section 5 describes the test location and the load and weather data recorded for a period of one year in this location and compares the results of the optimal system configuration obtained to the base case. Also, it examines the influence of seasonal variations in the test location on the dynamic performance of the optimal system and analyses the impact of the variations in size and cost of some system components on the optimal system. Finally, Section 6 is the concluding section of this paper where the key findings from the study are highlighted and future works recommended.

2. System description

The examined HRES integrates solar PV modules, horizontal axis wind turbines (WT), battery storage and Stirling engines (ST) and ORC back-up power block fired by biomass fuel (woodchips) as configured in Fig. 1. Here, the primary power sources are the PV and WT generators, while n-small split STs and battery banks are deployed to match the unmet electricity demand. The number of small STs that are switched on to fulfill the electricity demand is determined by a set of rules based on the net load in the system, i.e., difference between the electric load and the generated power from the PV and WT generators, the state of charge of the battery and the dispatch strategy. Four rules based on circuit charging and load following have been proposed to manage the flow of energy from the generating and storage units. The operating details of these dispatch modes will be discussed in the methodology. Also, in this system design, the battery system is the first priority to meet the deficit power, while the ST back-up will only be deployed when the battery system is unable to meet the net positive load. The back-up has two commitments in the circuit charging rule-based dispatch strategy: to charge the battery system with any excess power generated and to supply the net positive load in the system. Conversely, in the load following strategy, the back-up will simply follow the load and is not expected to charge the battery.

3. Components modelling and problem formulation

In this section, the modelling of the HRES and back-up components are presented. Further, the optimisation problem is formulated by considering technical, economic and environmental metrics.

3.1. Development of component models

This section presents the mathematical models for predicting the performance of the components of the proposed HRES. These models have been pivotal in formulating the objective functions deployed in the sizing optimisation of the HRES performed in this paper.

3.1.1. Photovoltaic modules

The hourly simulation of the power generation from one photovoltaic module can be obtained from [30]:

$$P_{pv}(t) = \eta_{PV} A_{PV} G_h(t) = P_{STC}\left[\frac{G_h(t)}{G_{STC}}\left(1 + \frac{\alpha}{100}(T_c(t) - T_a(t))\right)\right] F_{diss} \quad (1)$$

where $P_{\mathrm{STC}}(\mathrm{W})$ is the module maximum power at standard test conditions, $G_{\mathrm{h}}(\frac{W}{m^2})$ is the hourly global solar radiation, $G_{\mathrm{STC}}(\frac{W}{m^2})$ is the solar

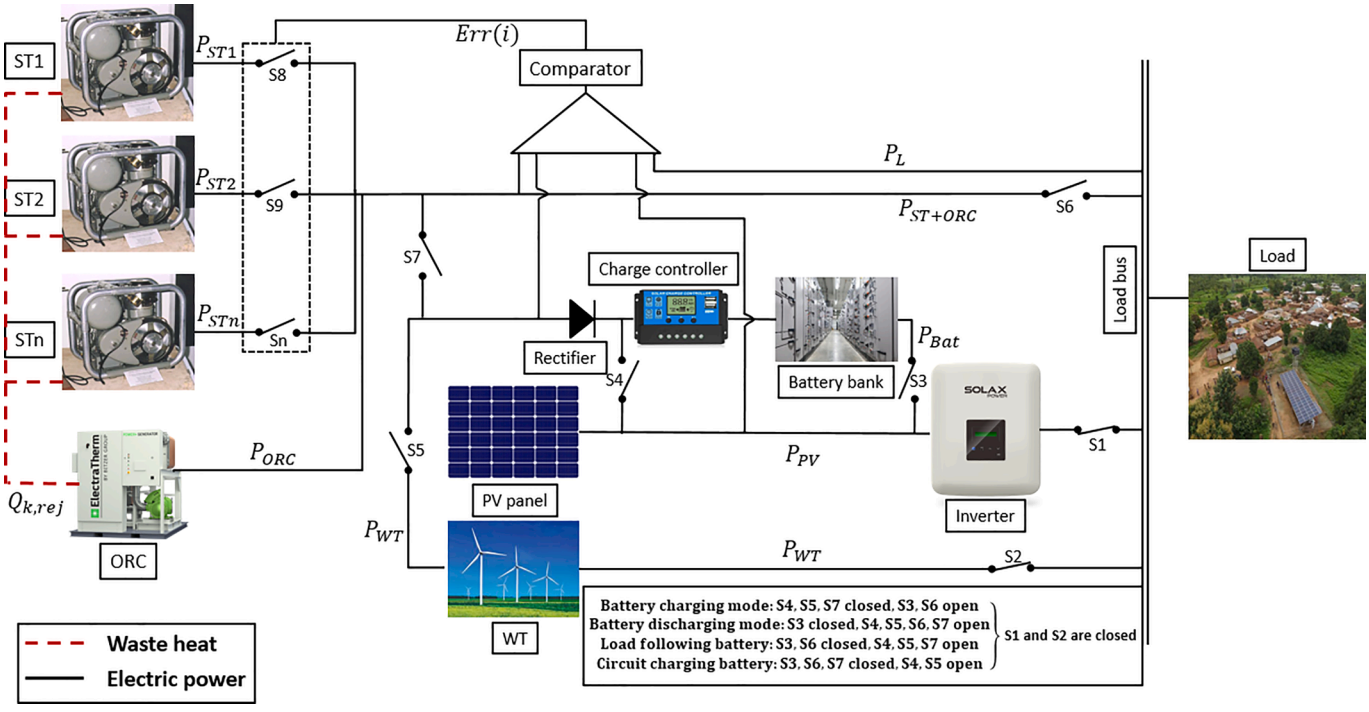

Fig. 1. Schematic of the HRES showing the operating modes and control strategies and the split of the Stirling engine.

radiation at the test conditions, α (%/°C) is the temperature coefficient, T_a (°C) is the ambient temperature and $F_{diss}(-)$ is a factor that accounts for power dissipation due to dirt, wires, modules mismatch, and other losses.

The cell temperature T_c (°C) is obtained from the following expression:

$$T_c(t) = T_a(t) + \left(\frac{NOCT - 20}{0.8}\right)\frac{G_h(t)}{G_{STC}} \tag{2}$$

where $NOCT$ (°C) is the nominal operating cell temperature and T_a (°C) is the ambient temperature.

Consequently, the power produced from the PV array at any time step, t, can be obtained as follows:

$$P_{array}(t) = IV = P_{pv}(t)N_sN_p \tag{3}$$

The number of PV modules arranged in series, N_s is given as a function of the bus voltage, V_{bus} and the rated voltage of the PV panel provided by the manufacturer, V_{PV}:

$$N_s = \frac{V_{bus}}{V_{PV}} \tag{4}$$

3.1.2. Wind turbines

The modelling of the power generated from the wind turbine is presented in this section. The actual power output from the wind turbine can be estimated from the power curve in Fig. 2 that is provided in the manufacturer's catalogue.

Based on the power curve provided by the manufacturer, the power that can be extracted from a moving stream of air at any given speed and hub height can be quantified directly using the following expression [15,32–33]:

$$P_{WT}(t) = \begin{cases} \frac{\nu^3 - \nu_c^3}{\nu_R^3 - \nu_c^3}.P_R\nu_C \le \nu \le \nu_R \\ P_R\nu_R \le \nu \le \nu_F \\ 0\nu \le \nu_C \ \ and \ \ \nu \ge \nu_F \end{cases} \tag{5}$$

where ν (m/s) is the wind speed in the test location, ν_C(m/s) is the cut-in wind speed, ν_R (m/s) is the rated wind speed, ν_F (m/s) is the cut-out wind speed and P_R(W) is the rated power of the turbine. The wind speed data at the location has been obtained from PV GIS [34] for a period of one year and was measured at 10 m hub height.

Regarding the stochastic nature of wind, the Weibull function has been deployed to estimate the frequency of the wind speed in the test location and it is given as:

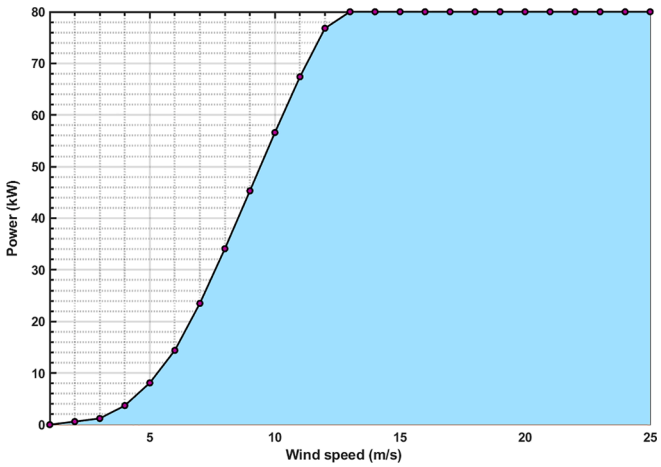

Fig. 2. Power curve of the Enercon E-18 wind turbine [31].

$$PDF_w(\nu) = \left(\frac{k}{\varsigma}\right)\left(\frac{\nu}{\varsigma}\right)^{k-1} exp\left(-\left(\frac{\upsilon}{\varsigma}\right)^k\right) \tag{6}$$

The Weibull shape factor, k can be obtained from the following expression [13]:

$$k = \left(\frac{\sigma(\nu)}{\bar{x}(\nu)}\right)^{-1.086} \tag{7}$$

And the wind scale index, ς is given as:

$$\frac{\varsigma}{\bar{x}(\nu)} = \left(0.568 + \frac{0.433}{k}\right)^{-1/k} \tag{8}$$

If k = 2 is substituted in Eq. (6), a Rayleigh function is obtained and is expressed as [13]:

$$PDF_r(\nu) = \frac{2\nu}{\varsigma^2} exp\left(-\left(\frac{\upsilon}{\varsigma}\right)^2\right) \tag{9}$$

The Rayleigh wind scale index can be estimated from [13]:

$$\varsigma = \frac{2}{\sqrt{\pi}}\nu_{ave} \approx 1.18\nu_{ave} \tag{10}$$

To obtain the wind speed at the hub height of the selected turbines, the following logarithmic law is employed [15,32]:

$$\nu_{hub} = \nu_r.\frac{\ln\frac{Z_{hub}}{Z_0}}{\ln\frac{Z_r}{Z_0}} \tag{11}$$

where ν_{hub} (m/s) is the wind speed at the hub height, Z_{hub} (m) is the desired hub height, Z_r (m) is the reference height, ν_r (m/s) is the wind velocity at the hub height, Z_0(m) is the surface roughness height.

3.1.3. Combined Stirling and ORC engine

As previously stated, this paper proposes a combined ST and ORC as the back-up to the HRES system, which is deployed to augment the electricity generation from the renewable generators. However, sole Stirling back-up is also proposed to compare results and assess the performance improvements. The power supplied by the combined ST + ORC back-up at any time step is determined by the availability of the renewable generators, the dispatch strategy and the state of charge of the battery. In this study, the biomass fuel consumption of the ST + ORC (or Stirling only), $FC_{STorST+ORC}$ (kg) will be determined from the energy balance of the heat engine and it has been expressed as:

$$FC_j(t) = \frac{3600P_{gen,j}(t)}{\eta_{combustor}HV_{woodchips}\eta_j}, j = STorST + ORC \tag{12}$$

where $P_{gen,ST+ORC}$ (W) is the power delivered by the back-up at a given time step, $\eta_{combustor}(-)$ is the efficiency of the biomass combustor, $HV_{woodchips}$ (J/kg) is the calorific value of woodchips and η_{ST+ORC} (−) is the electrical efficiency of ST + ORC back-up. The sole efficiency of the ST, combined efficiency of the ST and ST + ORC and combustor efficiency in Eq. (12) have been extracted from Ref. [29 35] and are given as 21%, 38% and 88%, respectively.

3.1.4. Diesel generator

The deployment of the ST in combined mode operation with an ORC has been proposed as the back-up to augment the net load in this HRES configuration. Nonetheless, the DG that has been popularly deployed as the back-up to HRES systems will be modelled here and will serve as the base case for benchmarking the performance improvements of the proposed back-ups. The power supplied by the DG at any time step is determined by the power generation capacity of the PV and WT, the load, the dispatch strategy and the SOC of the battery. It is modelled based on the hourly fuel consumption, FC_{DG} (l/Wh) and can be expressed as [15]:

$$FC_{DG}(t) = AP_{gen,DG}(t) + BP_{rated,DG} \quad (13)$$

The experimental constants, A (l/Wh) and B (l/Wh) in the above equation have been obtained from [8] and are given as 0.246 and 0.08415, respectively.

In addition, the greenhouse gas (GHG) emissions produced by the traditional DG back-up has been compared to that of the proposed biomass fired ST + ORC (and ST only) back-up. The GHG emitted by the DG or ST is determined according to the guidelines of the international panel on climate change (IPCC) and is given as [36]:

$$y^{F}_{GHG} = HV_F \chi^{F}_{GHG} FC_j, j = DGorST \quad (14)$$

where HV_F (J/kg) is the heating value of the fuel, χ^{F}_{GHG} (g GHG/J fuel) is the emission factor. The value of these constants have been extracted from [36–37] and presented in Table 1.

3.1.5. Battery storage

The battery is one of the dispatchable units deployed to meet the power deficits in the HRES configuration proposed here. In this study, the amount of energy the battery supplies or retains is determined by the excess power generated by the green generators, consumer electric load, power dispatching strategy, the state of charge (SOC) of the battery and the power generation from the back-up. At any time, t, the energy stored or released by the battery banks can be obtained from the following expressions:

Charging :

$$SOC(t+\Delta t) = \begin{cases} SOC(t) + \eta_{ch}\left(\frac{(P_{PV}(t) + P_{WT}(t) - P_L(t))}{V_{Bat}}\right)\Delta t/C_{Bat}, & LF \\ SOC(t) + \eta_{ch}\left(\frac{(P_{PV}(t) + P_{WT}(t) + P_{ST+ORC}(t) - P_L(t))}{V_{Bat}}\right)\Delta t/C_{Bat}, & CC \end{cases} \quad (15)$$

discharging :

$$SOC(t+\Delta t) = SOC(t) - \left(\frac{(P_L(t) - P_{PV}(t) - P_{WT}(t) - P_{ST+ORC}(t))}{\eta_{disch}.V_{Bat}}\right).\Delta t/C_{Bat} \quad (16)$$

where $\eta_{ch}(-)$, $\eta_{disch}(-)$, $V_{Bat}(V)$, $C_{Bat}(Ah)$ are the charging efficiency, discharge efficiency, voltage and nominal capacity of the battery, respectively, P_{PV} (W), P_{WT}(W), and P_{ST+ORC}(W) are the electric power produced by the PV, WT and ST + ORC, respectively, P_L(W) is the electric load, Δt(s) is the time interval. The time interval used in this study is 1 h. The specification and cost of the components of the system are given in Table 2.

Table 1
Constants for the evaluation of the GHG emissions [36–37].

Parameter	Value
Diesel	
Heating value (MJ/kg)	45
CO_2 Emissions factor (kg Co_2/ MJ)	0.074
N_2O Emissions factor (kg N_2O / MJ)	6.0×10^{-7}
Woodchips	
Heating value (MJ/kg)	19.2
CO_2 Emissions factor (kg Co_2/ MJ)	0.112
N_2O Emissions factor (kg N_2O / MJ)	4.0×10^{-6}

Table 2
Specification of the components of the HRES.

Component	Type	Specification	Value
Batteries (3 types) [38]	Hoppecke Sun AGM	Voltage, (V)	2
		Capacity, (Ah)	1120
	Hoppecke Sun AGM	Voltage, (V)	2
		Capacity, (Ah)	890
	Hoppecke Sun AGM	Voltage, (V)	2
		Capacity, (Ah)	620
Wind turbines (2 types) [31]	EWT DW 52–250 HH40	Cut-in speed, (m/s)	2.5
		Cut-out speed, (m/s)	25
		Rated speed, (m/s)	8
		Rated power, (kW)	250
	Enercon E-18	Cut-in speed, (m/s)	2.5
		Cut-out speed, (m/s)	25
		Rated speed, (m/s)	12
		Rated power, (kW)	80
PV modules (1 type) [39]	Canadian solar Hiku 7	Rated power, (W)	665
		Module efficiency, (%)	21.1
		Operating current, (A)	17.28
		Operating voltage, (V)	38.5
		Open circuit voltage, (V)	45.6
		Short circuit current, (A)	18.51
		NOCT, (°C)	42 ± 3
		Temperature coefficient, (%/°C)	−0.26
		Lifetime, (years)	20
MLPE inverter	AC rated	Capacity, (kVA)	48

3.2. Rule based dispatch strategies

The renewable generators in the proposed system rely strongly on the local weather data for their power generation. Consequently, the energy system cannot satisfactorily match the electric load demand at all times in a day. It has been mentioned that battery storage systems and ST + ORC back-up will be deployed to fulfill the electricity demand of the test location. Further, the battery storage system is designed to serve as the first priority to match the positive net load in the system, and when it is fully discharged, the ST + ORC back-up will be deployed. Additionally, four small STs have been proposed to minimise the hourly commitment of the back-up when deployed to supply the deficit power. The number of the small STs that are switched ON in parallel to augment the load is determined by the net load and the state of charge (SOC) of the battery.

Correspondingly, some set of rules are required to efficiently manage the flow of electricity in the proposed HRES. Therefore, the circuit charging (CC) with split ST option and the load following (LF) rule based energy management strategies have been proposed in this study. In these strategies, four rules based on if-then constructs are deployed to control the charging and discharging of the battery storage system, the dispatch of power from the back-up and the dumping of excess power from the WT and PV. These rules are formulated based on the state of charge of the battery at a given time step, $SOC(t)$ and the net load, $P_{net}(t)$, where,

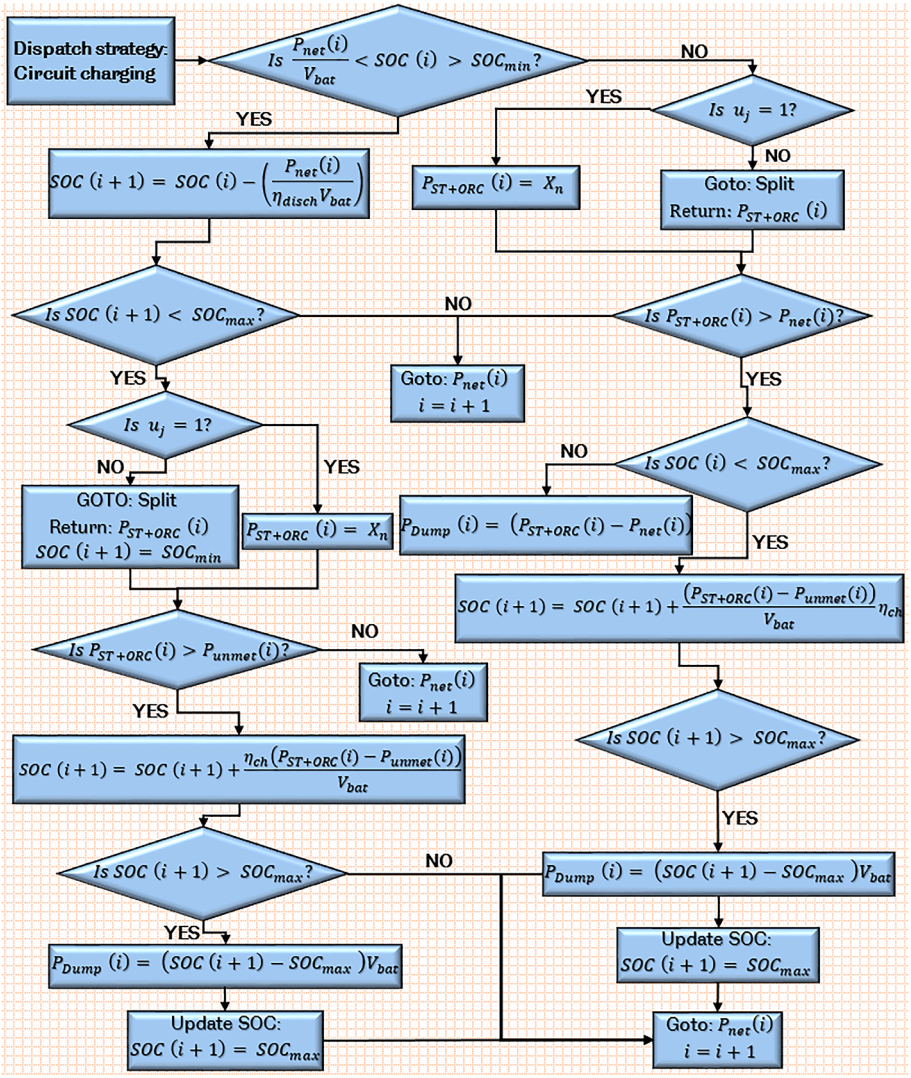

Fig. 3. Algorithm for circuit charging rule based dispatch strategy with split Stirling engine option.

$P_{net}(t) = P_L(t) - P_{PV}(t) - P_{WT}(t)$ [40]. Fig. 3 and Fig. 4 represent the algorithm for managing the energy flow in the HRES based on the following rules:

Battery charging mode: In this energy management strategy, two conditions control the charging of the battery.

Condition $1 : [P_L(t) - P_{PV}(t) - P_{WT}(t) < 0][SOC(t) < SOC_{max}]$When $P_{net}(t) < 0$, i.e., the total generation by the WT and PV exceeds the load and the charge stored in the battery is below its maximum capacity, the excess power generated is stored in the battery until it is fully charged. To achieve the charging of the battery by the excess power generated from the WT and PV, switches S4 and S5 in Fig. 1 are closed allowing the excess power to flow to the batteries.

Condition$2 : [P_{net}(t) > 0][P_{net}(t) < P_{ST+ORC}(t)][SOC(t) < SOC_{max}]$

In this case, the net load in the system is positive and the ST + ORC back-up is deployed to simultaneously augment the power and charge the BSS. Switches S4, S5 and S7 in Fig. 1 are switched on to accomplish this task in practice. Note that in the LF strategy, only the excess power from the renewable generators is deployed to charge the batteries; hence, this condition is not applicable in this mode.

Power dumping mode: Similarly, additional two conditions, which are mirrored from the charging mode are implemented here to dump the excess power produced in the system.

Condition$1 : [P_L(t) - P_{PV}(t) - P_{WT}(t) < 0][SOC(t) = SOC_{max}]$

This rule controls the dumping of excess power produced from the renewable generators. Therefore, if there is negative net load in the system and the battery is fully charged, the excess power is dumped via resistive loads.

Condition$2 : [P_{net}(t) < 0][P_{net}(t) < P_{ST+ORC}(t)][SOC(t) = SOC_{max}]$

Condition 2 controls the dumping of excess power produced from the ST + ORC back-up after fulfilling its commitments to augment the power supply in the system and charge the batteries. Any excess power produced at this point is dumped via resistive loads. Note that in the LF strategy, the back-up follows the load strictly; thus, this condition does not apply in this approach.

Battery discharging mode: *Condition* $: [P_{net}(t) > 0][SOC(t) > SOC_{min}]$ When the total generation from the WT and PV is insufficient to match the load, i.e., there is positive net load in the system and the battery is above its minimum SOC, it is switched on to supply the load. Therefore, switch S3 is closed and this will allow the battery discharge its power through the inverter to the load bus. However, the battery is not expected to discharge power below its minimum SOC: SOC_{min}.

Back-up power dispatching mode: The dispatch of power from the back-up is determined by the net positive load in the system. Additionally, this study proposed four-split Stirling engines back-up. To compare performance improvements between split ST and one big ST, a control vector, u_j has been deployed to switch from one ST to split ST as seen in Fig. 3 and Fig. 5. So, if $u_j = 1$, one big ST is deployed in the simulation of the dispatch strategy, otherwise, small split STs are

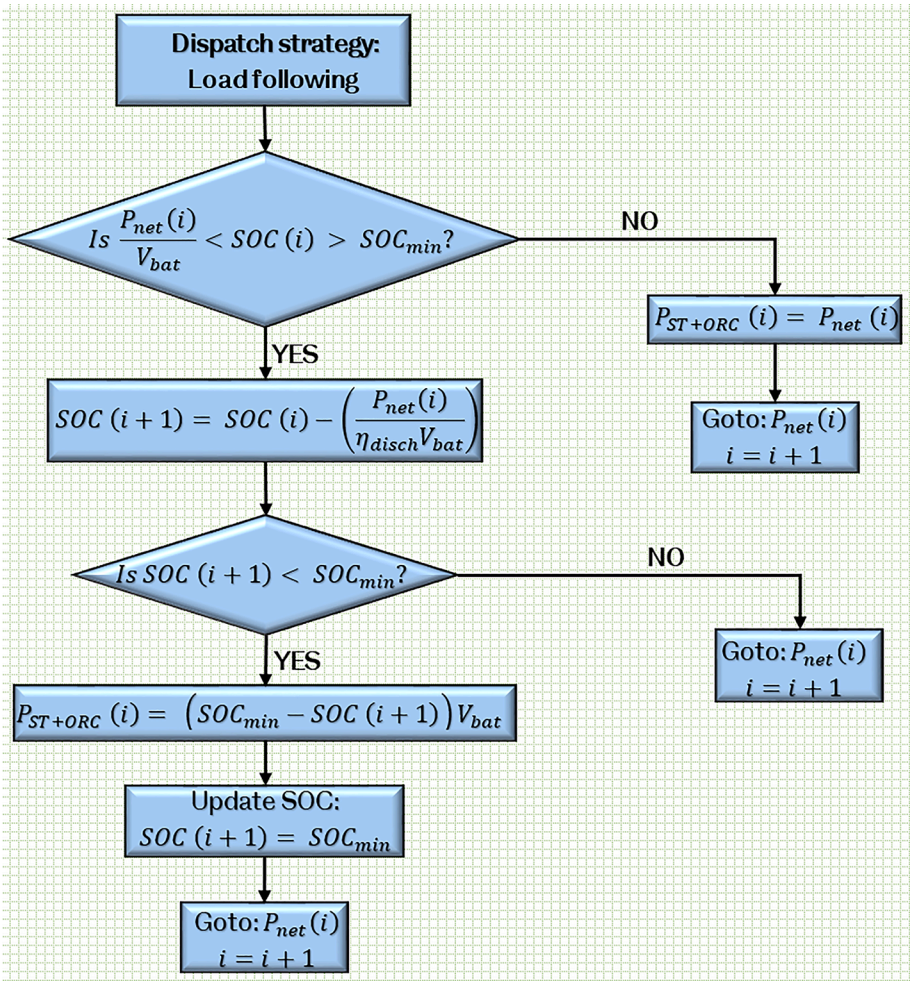

Fig. 4. Algorithm for load following dispatch strategy.

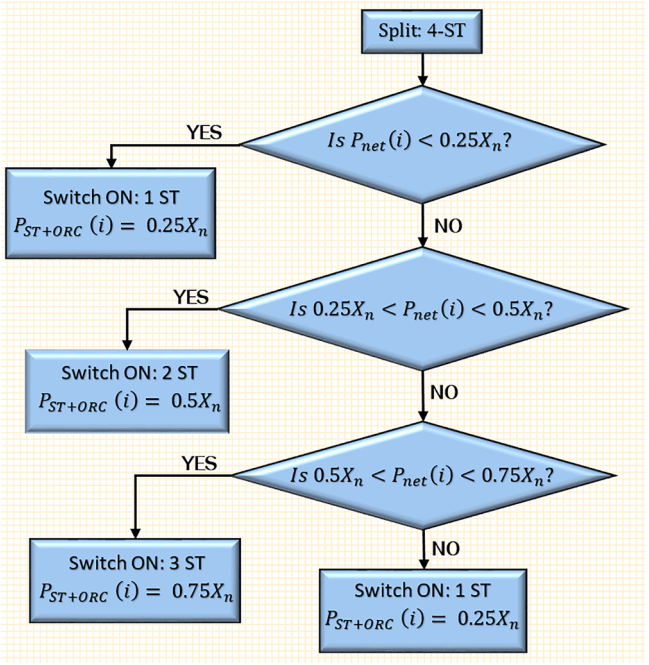

Fig. 5. Algorithm for implementing the power dispatch from split Stirling engines.

deployed. Note that X_n in these figures is the total capacity of the back-up system. Also, the split ST option does not apply in the LF strategy, where the back-up is expected to follow the load (See, Fig. 4. Based on these two factors, the power dispatch by the back-up is controlled by the following conditions.

o $condition1 : [P_{net}(t) > 0\,][u_j = 1]$

In this case, the ST + ORC back-up is deployed to match the unmet load while operating at its rated capacity. This is achieved by closing all the Switches, S8 to S11 controlling the small ST. In the load following strategy, the ST + ORC back-up will operate mostly below its rated capacity to follow the load.

$Condition2 : [P_{net}(t) > 0\,][P_{net}(t) \le P_{1-ST}\,][u_j = 2]$

Here, one small ST is deployed if the net load in the system is positive but below the capacity of one small ST. Therefore, one of the STs in the 4-split STs back-up is switched ON by closing any of the switches S8 to S11.

$Condition3 : [P_{net}(t) > 0\,][P_{1-ST} < P_{net}(t) \le P_{2-ST}\,][u_j = 2]$

In contrast to condition two, two of the STs are powered ON here to meet the deficit power, because it is above the capacity only one ST in the split can handle. Thus, any two switches from switches S8 to S11 are closed to power ON two STs to operate in parallel and supply the unmet load.

$Condition4 : [P_{net}(t) > 0\,][P_{2-ST} < P_{net}(t) \le P_{3-ST}\,][u_j = 2]$

Here, three-split STs are simultaneously deployed to match the positive net load in the system by switching ON any of the three switches

controlling the split STs (S8 – S11). Obviously, two-split STs are unable to handle the deficit power here.

$Condition5: [P_{net}(t) > 0][P_{net}(t) \geq P_{3-ST}][u_j = 2]$

If the deficit power in the system is higher than that can be handled by 3-split ST back-ups, all the switches controlling the split STs are closed and the engines will be powered ON simultaneously. Condition 5 is similar to the first condition. These rules have been deployed to manage the flow of energy in the HRES in the inner loop of the sizing optimisation procedure and fulfil the hourly commitments of its components.

3.3. Problem formulation

The formulation of the optimisation problem is performed in this section. The metrics for evaluating the design of the HRES are first presented and the optimisation problem is developed.

3.3.1. Evaluation metrics

Based on the reviewed literature and the objectives of this study, the loss of power supply probability (LPSP), levelised cost of energy (LCOE) and dumped power have been selected as the metrics for undertaking the sizing optimisation of the HRES.

(a) Levelised cost of energy

The levelised cost of energy (LCOE) is an economic indicator that quantifies the cost of the energy produced from the system over its life cycle. It is the ratio of the net present cost (NPC) for generating power from the system to the total electricity demand [41]. The NPC comprises the installation and acquisition cost of the components, the operating and maintenance (O&M) cost, the replacement cost of components, and the cost of fuel for the entire life of the system converted back to the initial time of purchase of the components (year 1). Considering the interest and inflation rates, the NPC can be expressed as [15,33]:

$$NPC = \sum_{j} \left(Annc_{I\&A,j} + Annc_{O\&M,j} + Annc_{rep,j} + Annc_{fuel,j}\right), j \equiv PV, WT, Bat, ORC, ST, Inv \tag{17}$$

where the annualised acquisition and installation cost, $Annc_{\mathrm{I\&A}}$, annualised operating and maintenance cost, $Annc_{\mathrm{O\&M,j}}$, annualised replacement cost, $Annc_{\mathrm{rep,j}}$ and annualised fuel cost, $Annc_{\mathrm{fuel,j}}$, respectively of a component, j are given by:

$$Annc_{I\&A} = \sum_{j} C_{I\&A,j} \times N_j \tag{18}$$

$$Annc_{O\&M} = \sum_{i=1}^{n_{system}} C_{O\&M,j} \left(\frac{(1+r_{inf})^{n_{system}}}{(1+r_{int})^{n_{system}}}\right) \tag{19}$$

$$Annc_{rep} = \sum_{m=1}^{N_{rep,j}} C_{I\&A,j} \left(\frac{(1+r_{inf})^{m.n_j}}{(1+r_{int})^{m.n_j}}\right) - C_j \left(\frac{n_j - \left(n_{system} - N_{rep,j} n_j\right)}{n_j}\right) \left(\frac{(1+r_{inf})^{n_{system}}}{(1+r_{int})^{n_{system}}}\right) \tag{20}$$

Table 3
Market price of the system components.

Component	Description	Value
Acquisition and installation cost		
Wind turbine	Enercon E-18 per kW (US $)	700 [42]
	EWT DW 52–250 per kW (US $)	700 [42]
Solar PV	Hiku 7 cost per panel (US $)	987 [39]
Battery	Hoppecke 620 Ah (US $)	350 [38]
	Hoppecke 890 Ah (US $)	405 [38]
	Hoppecke 1120 Ah (US $)	530 [38]
Stirling engine	Acquisition cost per kW (US $)	500 [43]
ORC engine	Acquisition cost per kW (US $)	1700 [44]
Diesel generator	Acquisition cost per kW (US $)	1000 [18]
MLPE inverter	Cost per kW (US $)	120 [42]
Operating and maintenance cost		
Fuel cost	Nigerian woodchips (US $/tonne)	85
Fuel cost	Diesel fuel (US $/liter)	0.689
Wind turbine	Maintenance cost per kW (US $)	0.02 [7]
PV	Maintenance cost per kW (US $)	0.005 [7]
Stirling engine	Maintenance cost per kW (US $)	0.0095 [43]
ORC engine	Maintenance cost per kW (US $)	0.008 [44]
Diesel generator	Maintenance cost per per kW (US $)	0.064 [18]
Financial assumptions		
Interest rate	Bank interest rate on capital	12.5
Inflation rate	Inflation rate on capital	15
ST life	Lifespan of ST (years)	10
ORC life	Lifespan of ORC (years)	10
Diesel generator	Life span of DG (years)	5
Plant life	Life span of the system	20

$$Annc_{fuel,j} = \sum_{i=1}^{n_{system}} C_{fuel,j} \left(\frac{(1+r_{inf})^{n_{system}}}{(1+r_{int})^{n_{system}}}\right) \tag{21}$$

The cost of fuel, $C_{\mathrm{fuel,j}}$ is given as:

$$C_{fuel,j} = \left\{ c_{fuel,j} \sum_{t=0}^{8760} FC_{i=DG,ST,ST+ORC}(t) \;, j = dieselorwoodchips \right. \tag{22}$$

Thus, the levelised cost of energy is therefore given as [9]:

$$LCOE = \frac{NPC}{\sum_{t=1}^{t=8760} P_L(t)} \tag{23}$$

The cost data of the components and other financial assumptions used to evaluate the economic objective in this study are provided in Table 3.

(b) Loss of power supply probability

The loss of power supply probability (LPSP) is a statistical parameter that assesses the reliability of the renewable energy resources in meeting the electricity demand of the design location. A low LPSP indicates that the renewable energy resources are sufficiently matching the load requirements. On the contrary, high LPSP implies that the renewable energy resources are unable to meet the energy demand of the location and as a result, the system may rely more on the back-up power sources to

match the demand. While it is desirable to have low LPSP, i.e., high penetration of renewable energy resources, it is important to ensure that the system is not oversized to avoid excessive dumping of energy. The LPSP has been expressed as follows [9,41]:

$$LPSP = \frac{\sum_{t=1}^{t=8760}\left(P_L(t) - (P_{PV}(t) + P_{WT}(t)) + P_{ST+ORC}(t) + P_{Bat,SOC^{min}}\right)}{\sum_{t=1}^{t=8760} P_L(t)} \quad (24)$$

(c) Dumped power

The dumped power quantifies the amount of excess electricity being generated by the HRES that is dumped via resistive loads. The generation of excess power is inevitable in a HRES because PV and WT power generation is at variance with the electricity consumption. Hence, excess power is generated from the HRES, which is largely an evidence that the system is over-sized and this results in high energy cost. On the other hand, power curtailment with the intention of reducing dumped power, results to high energy cost and increased emissions, because of the increased reliance on the DG to fulfill the net load. It is, therefore, important to minimise the dumped power from the renewable generators in a HRES, while simultaneously minimising the deployment of the back-up. The dumped power from the HRES can be obtained as follows:

$$P_{Dumped} = \begin{cases} \sum_{t=1}^{t=8760} \left((P_{PV}(t) + P_{WT}(t)) - P_L(t)\right), (P_{PV}(t) + P_{WT}(t) > P_L(t) \\ \qquad\qquad (P_{ST+ORC}(t) - P_L(t)), P_{ST+ORC}(t) > P_L(t) \end{cases} \quad (25)$$

3.3.2. Optimisation problem

The mathematical formulation of the evaluation metrics has been undertaken and the expressions presented in Eq. (17) – (25). For a predefined load profile of the consumer, the optimisation problem aim to determine the optimal number and types of system components that will minimise the levelised cost of energy (LCOE), loss of power supply (LPSP), dumped power (P_{Dumped}) and greenhouse gas (GHG) emissions (y^{F}_{GHG}) over the plant life of 20 years. This section presents the mathematical formulation of the objective functions and the constraints that must be satisfied to select an optimum system configuration.

(a) Optimisation function

The formulated evaluation metrics are the mathematical expressions of the objective functions. The optimisation problem is formulated as a multi-objective problem aimed at simultaneously minimising the three objective functions and is presented as follows:

$$minimise f(X) = f_i(X), f_j(X), f_k(X) i \neq j \neq k \forall : g_i(X) = 0 and h_i(X) \leq 0 \quad (26)$$

$$X \in \{X_i, i = 1, 2, \cdots\cdots n-1, n\} \quad (27)$$

where i, j, $k \in \{1,2,3\}$, the objective functions, $f \in \{\text{LCOE}, \text{LPSP}, \text{P}_{\text{dumped}}\}$, g_i are the equality constraints, h_i are the inequality constraints and X are the decision variables. $X_1 =$ number of PV modules in parallel, $X_2 =$ number of wind turbines, $X_3 =$ type of wind turbine, $X_4 =$ the capacity of the back-up power block and $X_5 =$ number of batteries in parallel and $X_6 =$ type of battery. Here, two wind turbine types of different specifications and from different manufactures have been selected while three battery types of different capacities were selected.

(b) Constraints

The optimal solution must satisfy the following conditions:

(i) Energy generation and consumption matching: for the worst days, i.e., days characterised by bad weather and poor energy generation from the renewable energy sources:

$$\sum_{t=1}^{t=24} (P_{PV}(t) + P_{WT}(t)) \geq \sum_{t=1}^{t=24} (P_L(t)) \quad (28)$$

Note that the total generation on a day marked by heavy thunderstorms will be insufficient to meet the demand for obvious reasons.

Table 4
The upper and lower bounds of the decision variables.

Parameter	Lower bound	Upper bound
Number of PV in parallel (-)	1	1200
Number of type 1 wind turbine (-)	0	5
Number of type 2 wind turbine (-)	0	8
Wind turbine type (-)	1	2
ST + ORC capacity (kW)	140	220
Number of batteries in parallel (-)	1	30
Battery type (-)	1	3

Besides, PV and WT are only able to generate power for some hours even on a bright day, because of the periodic and stochastic nature of solar and wind resources. Hence, back-ups cannot be dispensed in these systems.

(ii) Back-up power and demand matching: total capacity of the ST + ORC should not go below a threshold,

$$\sum_{i=1}^{n} P_{ST+ORC}(t) \geq x_f P_L \quad (29)$$

where $x_f(-)$ is the minimum capacity threshold of the back-up.

(iii) Battery storage and discharge limits: the maximum depth of discharge (DOD) of the battery has been supplied by the manufacturer. In this study, the battery is only expected to discharge power when its capacity is above $SOC_{\min}$. By contrast, in the charging mode, the power stored in the battery is not expected to exceed $SOC_{\max}$.

$$(1 - DOD)\left(\frac{N_{Bat}}{N_{Bat,S}}\right) C_{Bat,max} \leq C_{Bat}(t) \leq \left(\frac{N_{Bat}}{N_{Bat,S}}\right) C_{Bat,max} \quad (30)$$

where $N_{\text{Bat,S}} = \frac{V_{\text{Bus}}}{V_{\text{Bat}}}$ is the number of batteries in series, $V_{\text{Bus}}(\text{V})$ is the bus voltage, $C_{\text{Bat,max}}(\text{Ah})$ is the maximum capacity of the battery. Furthermore, the power stored in the battery or discharged from the battery must not exceed the capacity of the battery

$$\text{Batterydischargemode} : P_{disch,Bat}(t) \leq \left(\frac{N_{Bat}}{N_{Bat,S}}\right) C_{Bat,max} V_{Bat} \quad (31)$$

$$\text{Batterychargemode} : P_{ch,Bat}(t) \leq \left(\frac{N_{Bat}}{N_{Bat,S}}\right) C_{Bat,max} V_{Bat} \quad (32)$$

(iv) Battery capacity: here the battery storage has been designed to handle mainly the constant base load demand in the morning and the transient load at peak hours. Hence, a constraint to ensure the battery capacity is sufficient to match the base load when it is in the power discharge mode has been introduced into the system sizing optimisation:

$$\text{Batterycapacity} : N_{Bat}.C_{Bat,max} \geq z_f P_L \quad (33)$$

where $z_f(-)$ is the minimum threshold of the capacity of the BSS.

(v) Limits on components: upper and lower limits have been set on the number of components and types of components. In the case of the type of components, the absolute value of the random number generated within the given range represents the type of the component, j selected and this will prompt the release of the corresponding component data.

Table 5
Specifications of the GA operator.

Parameter	Value
Population size (-)	250
Population type (-)	Double vector
Pareto fraction (-)	0.5
Maximum generation (-)	500
Cross-over operator (-)	Intermediate
Cross-over fraction (-)	0.8
Hybrid function (-)	fgoalattain

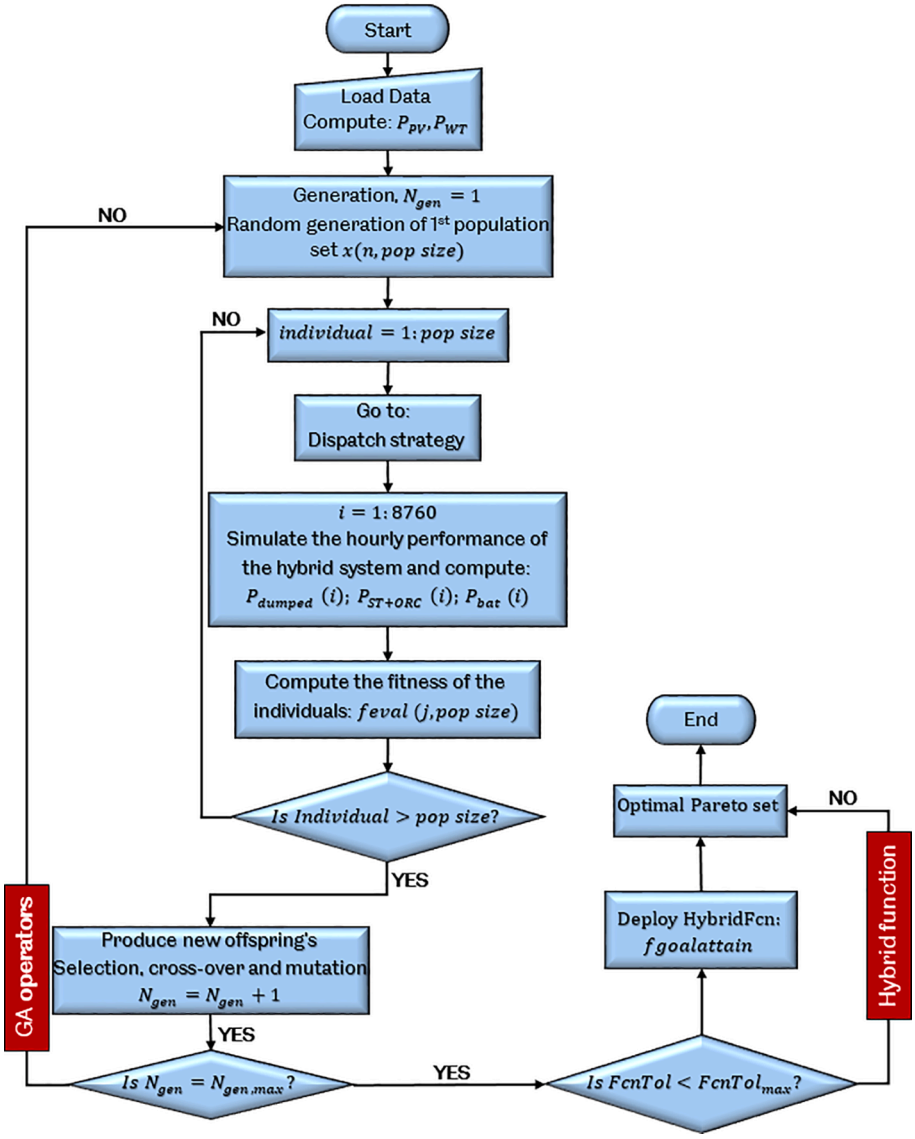

Fig. 6. Algorithm for the HRES system sizing optimisation.

$$X_{j,min} \leq X_j \leq X_{j,max} \tag{34}$$

where $X_{\mathrm{j,min}}(-)$ is the lower bound, $X_{\mathrm{j,max}}(-)$ is the upper bound and $X_{\mathrm{j}}(-)$ is the number or type of component, j. The range of values of the decision variables are given in Table 4.

4. Solution approach

The solution approach to the optimisation problem that has been earlier formulated is presented in this section. As can be seen from the models developed in Section 3.1, the power generation from the HRES components is strongly dependent on the unpredictable weather and electricity demand data, which introduces some complexity in the optimisation problem. Consequently, different heuristic tools have been deployed to solve optimisation problems that involve HRES sizing including, genetic algorithm (GA) [3,7–8,45], particle swarm optimisation (PSO) [17,24,46], fruit fly optimisation [12], grasshopper optimisation [6,18] and multi-objective self-adaptive differential evolution (MOSaDE) [9]. GA has been widely deployed in sizing HRES among all the heuristic tools. GA is a robust evolution algorithm with the advantage of avoiding getting trapped in the local optima; however, like most memetic algorithms, it does not converge at the global optimal [5,8]. This problem is overcome by hybridising the GA with other classical optimisation tools. Therefore, the elitist Pareto front non-dominated sorting genetic algorithm (NSGA-II) hybridised with a classical optimisation search tool was deployed in solving the multi-objectives optimisation problem. The details of the GA operators are presented in Table 5.

The NSGA II is an elitist optimisation method that emphasises only the non-dominated solutions while ensuring the diversity of the population is preserved [47]. It achieves this by combining the population of the parent and offspring in a given generation and groups them into non-dominated classes. Then, it populates the spaces in the Pareto front of the new generation with strong individuals from the respective classes and deletes individuals which cannot be accommodated in the Pareto front [47]. On the other hand, fgoalattain is a goal attainment classical optimisation method that works with the weighted approach. The weights are computed from the solutions generated in the last generation of the GA approach.

The algorithm for implementing the solution to the optimisation problem is presented in Fig. 6. Matlab Simulink blocks of the PV and WT generators were built with the models presented in Section 3.1, for the hourly simulation of the renewable generators. These Simulink blocks rely on the local weather data (solar irradiance, wind speed and temperature) and the manufacturers' data of the components to simulate the

power generation of the renewable generators. Therefore, as seen in Fig. 6, the load and weather data (solar irradiance, wind speed and temperature) for a period of one year are fed into the Simulink blocks.

These weather and load data and system configuration data (number and types of component) encoded in the initial random population of individuals generated by the GA, have been used to compute the hourly power generation from the PV and WT generators. The initial population of individuals, Pop_i in the first generation, G_i comprises n different configurations of the HRES that need to be evaluated to obtain the configuration that best satisfies the objectives and meets all the constraints. It is represented in a vector form as:

$$Pop_i = \begin{bmatrix} X_1^1 X_2^1 X_3^1 X_4^1 X_5^1 X_6^1 \\ X_1^2 X_2^2 X_3^2 X_4^2 X_5^2 X_6^2 \\ X_1^3 X_2^3 X_3^3 X_4^3 X_5^3 X_6^3 \\ \cdots\cdots \\ \cdots\cdots \\ \cdots\cdots \\ \cdots\cdots \\ X_1^n X_2^n X_3^n X_4^n X_5^n X_6^n \end{bmatrix} = \begin{bmatrix} X_1 \\ X_2 \\ X_3 \\ . \\ . \\ . \\ . \\ X_n \end{bmatrix} \quad (35)$$

where X is a vector representing the genotype of each individual in the population.

Then, the net load in the system is determined and based on its magnitude, the optimisation algorithm will implement the rule-based dispatch strategies described in Section 3.2 and obtain $P_{disch,Bat}(t)$, $P_{ch,Bat}$, $P_{ST+ORC}(t)$, $P_{Dumped}(t)$ and $SOC(t)$ for every hour in one year ($t = 8760$). Thereafter, the objective functions, i.e., fitness of the individuals are computed. Subsequently, the GA operators (selection, cross-over and mutation) are deployed to generate the parent generation and the entire process is repeated until the stopping criteria is met.

In the case of the simultaneous optimisation of two or more conflicting objective functions, the NSGA-II presents the optimal system configuration in the form of a Pareto front that contains non-dominated optimal solutions. Thus, it is necessary to deploy a multi-criteria decision making (MCDM) tool to select the best system configuration from the Pareto set. This paper used the technique for order preference by similarity to ideal solution (TOPSIS), which has been described in [48] and was deployed for the first time in sizing HRES by Perera et al. [49], to select the best optimal system configuration. The TOPSIS decision making process is described in Fig. 7. To obtain the weight for the objective functions, a decision matrix is developed based on a scoring criteria and then solved to determine the maximum eigenvalue ($max|det(A - \lambda I) = 0|$) and corresponding eigenvector ($(A - \lambda I) = 0$). The scoring criteria [54] and the resulting decision matrix are presented in the Appendix. The TOPSIS MCDM selects the best system configuration from the Pareto set of optimal solutions:

$$X^{best} = \left[X_1^{best} X_2^{best} X_3^{best} X_4^{best} X_5^{best} X_6^{best}\right] \quad (36)$$

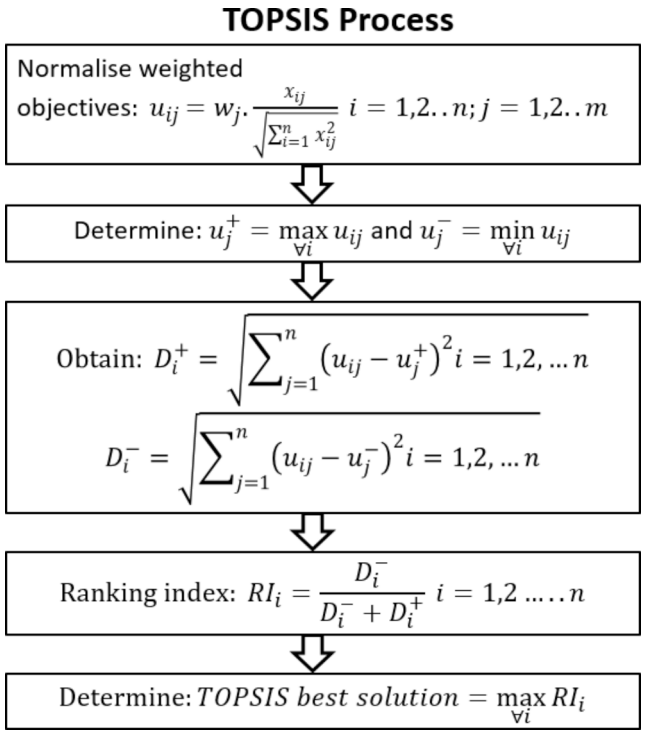

Fig. 7. TOPSIS decision making process.

5. Results and discussion

This section evaluates the weather data in the proposed test location. It also presents the results obtained from the sizing optimisation of the system and undertakes comparative analysis of the optimal configurations to highlight the impact of split ST and combined ST + ORC back-up in circuit charging and load following dispatch modes. Finally, the section discusses the influence of seasonal variations and changes in the cost and size of components on the optimum system configuration.

5.1. Design location

The proposed hybrid energy system sizing optimisation has been undertaken with the data from a remote location in the coastal area of Southern Nigeria (Onye-Okpan community; latitude: 5.976515° N and longitude: 8.47067° E) with 500 households and situated seven kilometers away from the nearest electrified town. This location is notable for medium scale commercial activities involving the processing and trading of agricultural products (yam, cassava and cocoa beans), welding and fabrication of farm implements, and other artisan related activities [50]. It requires 230 kW (60 kW for households and 170 kW for commercial activities and total daily consumption of 2.952 MWh/day) to meet the daily electric load of the residents.

5.2. Load and weather data of the design location

The hourly load data for this location is presented in Fig. 8 and it also shows the electricity consumption for one representative day. As it is seen from the data, the daily energy consumption is 2.952 MWh/day with a peak load of 219.19 kW recorded at 21:00 h. At the beginning of

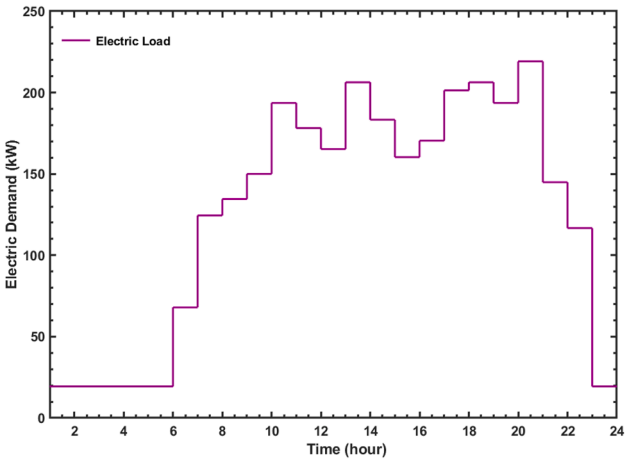

Fig. 8. Hourly electricity consumption at the design location [50].

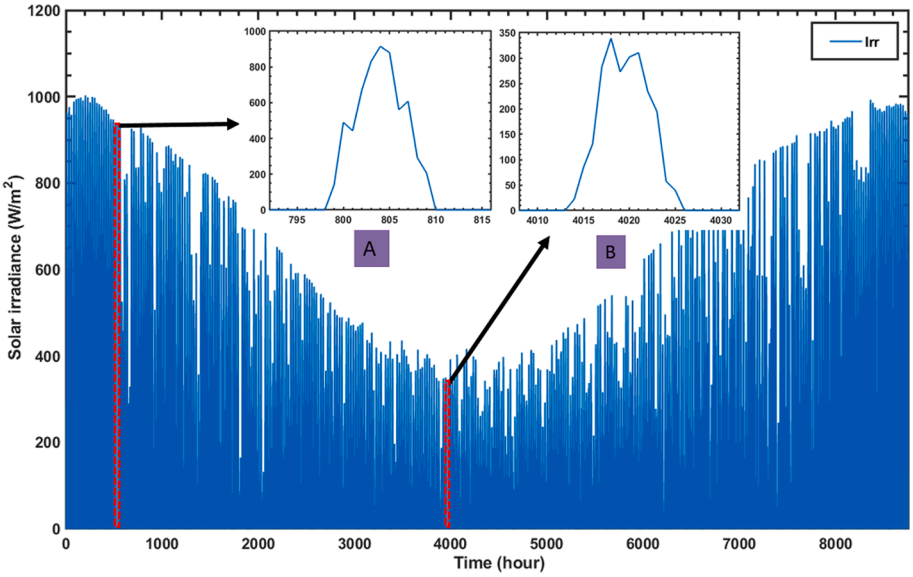

Fig. 9. Hourly solar irradiation at the design location [34].

the day, the electricity consumption is about 20 kW, it starts to increase from the dawn and reaches the first peak at 11:00 h. Subsequently, the electricity consumption fluctuates around this value with increased productive activities.

In Fig. 9, the global solar irradiance of the location is depicted for a typical meteorological year. The daily solar irradiance for two typical days in the dry and wet seasons that are characterised by bright weather with a clear sky and stormy weather have been highlighted in Fig. 9 as A and B, respectively. It can be observed that, the solar insolation at the location records a high value of about 900 W/m^2 on a bright day, while the peak insolation on a typical stormy day with poor weather is about 330 W/m^2. Furthermore, this location enjoys a daily average sunshine of 7 h with an average solar insolation of 4.52 kWh/m^2. This amount of solar insolation is sufficient to support a stand-alone hybrid renewable energy system [51].

Fig. 10 depicts the hourly average ambient temperature and solar insolation per square area of the PV surface that is recorded in a period of one year, in the test location. As Fig. 10 (a) shows, high hourly average solar insolation between 500–800 W/m^2 is experienced in the mid-day from late October to early March, which are the months in the dry season. It is seen that in the rainy season (April – October), the average hourly solar insolation reduces in intensity as expected, due to the stormy weather.

Similarly, in Fig. 10 (b) that shows the average hourly ambient temperature of the test location, the ambient temperature starts to increase just towards the end of the rainy season. It is seen to attain a peak of 31 °C in December, before it starts to drop albeit, slowly. Relative stability in the ambient temperature is notable from late January to early May. It is also evident, that the rainy season is characterised by low ambient temperature due to cloud cover, and this explains the low irradiance observed for the rainy season months.

Conversely, Fig. 11 depicts the annual hourly wind speed in the test location measured at 50 m hub height. As seen in Fig. 11, sharp variation in the wind speed in the test location can be observed all year round,

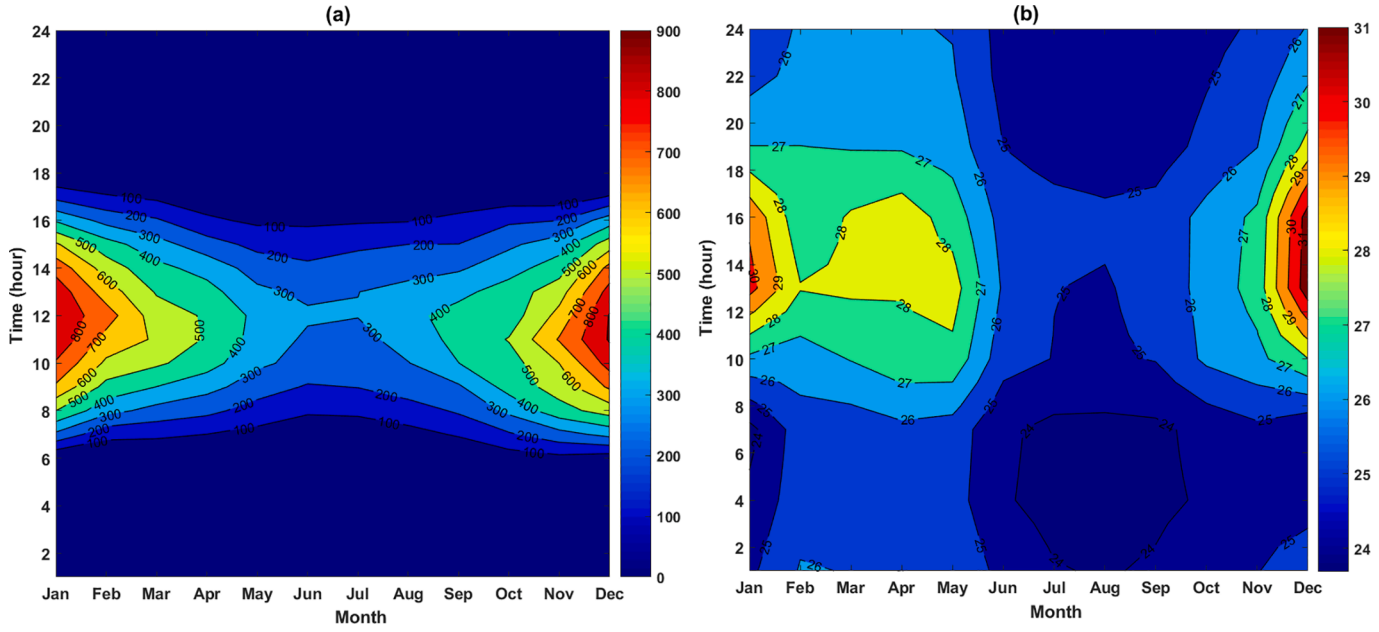

Fig. 10. Heat map of (a) average solar irradiance, G_o (W/m^2) and (b) average daily hourly ambient temperature, T_a (°C) in the test location.

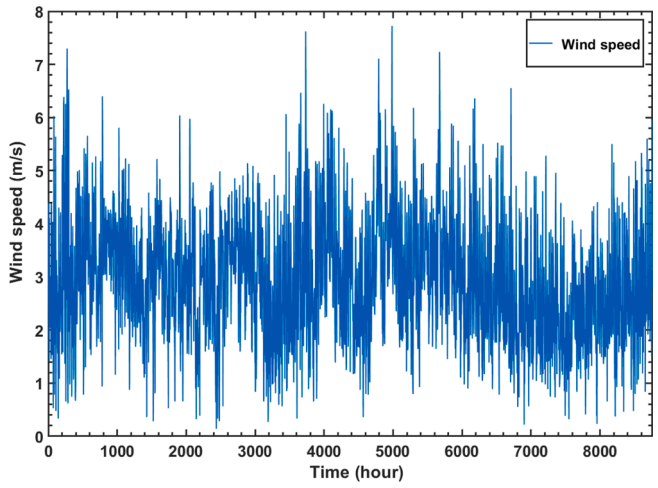

Fig. 11. Hourly wind speed at the design location [34].

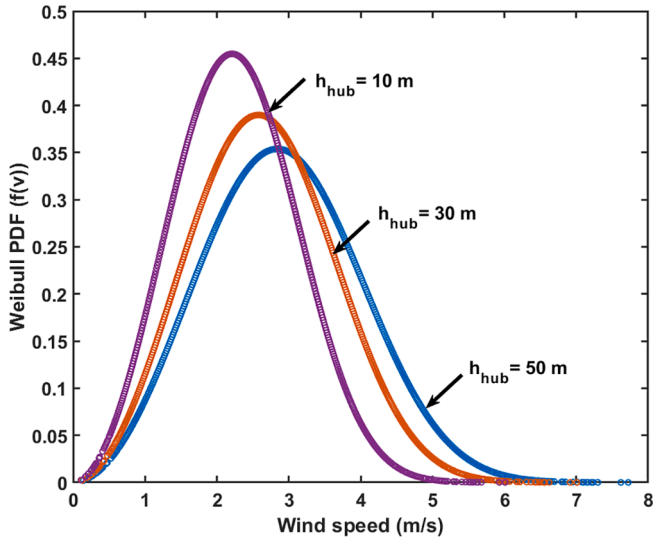

Fig. 12. Weibull distribution of wind speed in the test location for a period of one year.

although not as drastic as in the case of the solar insolation. From the seasonal perspective, high wind speed is notable in the rainy season where some months recorded hourly wind speeds of 7.5 m/s.

Regarding the stochastic behavior of wind, the Weibull distribution of the wind speed in the test location is shown in Fig. 12 for different hub heights. Fig. 12 shows that wind speed of 3.0 m/s has the highest frequency of occurrence in the year at 50 m hub height. With the decrease in the hub height, the peak Weibull frequency increases, while the average wind speed decreases. Meanwhile, wind speed v > 3.5 s is observed for more than 65 % of the curve at the design hub height of 50 m. Fig. 13 is the hourly average wind speed in the location for the different months in a year. It is evident that there are two peak wind speed periods between May – June and August – September with an hourly average wind speed of about 3.5–4 m/s. However, it is evident that all the months in the year experienced periods of average wind speed of 3.0 m/s.

The high wind speed periods experienced during the rainy season, which doubles as the period in the year with poor solar insolation, highlights the complementarity that exists between wind and solar energy resources; hence, the motivation for their hybridisation. Finally, the test location has a considerable share of solar and wind energy resource to support the siting of a HRES.

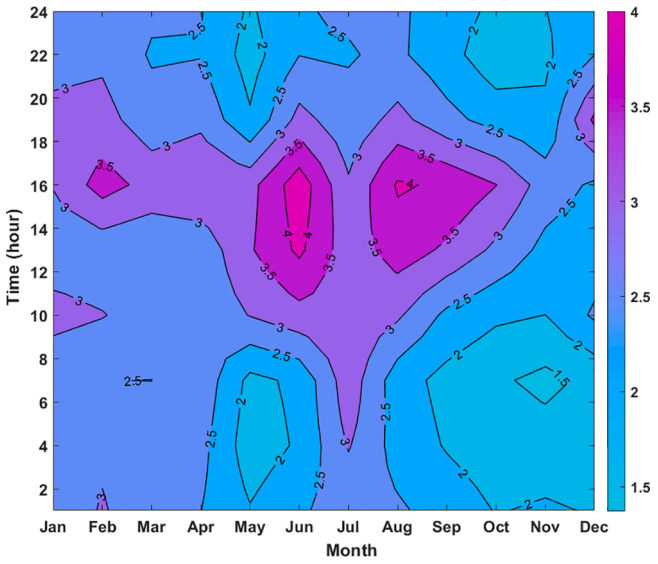

Fig. 13. Heat map of average daily hourly wind speed at 30 m hub height in the test location.

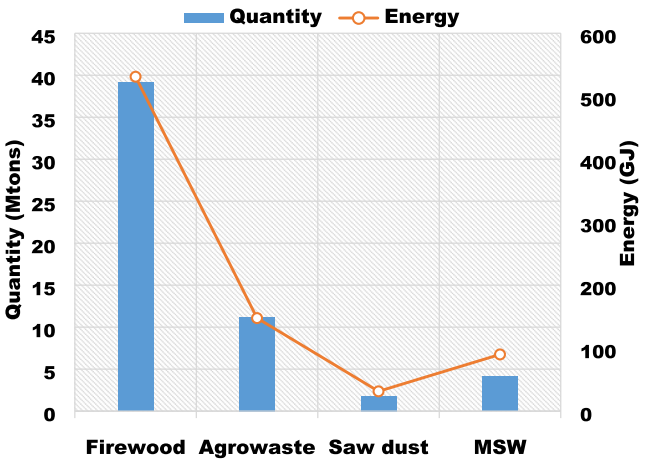

Fig. 14. Estimates from different sources of biomass in Nigeria [52].

Fig. 14 represents the estimates of the quantity and energy content of some biomass resources in Nigeria. It is evident that more than 70% of the available biomass resource in Nigeria is derived from wood [52]. This under-utilised biomass resource has an estimated energy content of over 500 GJ and are commonly found in remote locations. It is, therefore, a promising fuel to power a programmable generator that can be deployed to ensure the reliability of a hybrid system designed to meet the energy needs of a remote off-grid location.

5.3. Results of optimal hybrid system configurations

In this paper, several HRES cases based on the two main dispatch strategies examined have been formulated to compare results to the base case: HRES with DG back-up. The Pareto optimal set, which are a combination of the number and types of the components of the proposed HRES and the formulated cases that simultaneously minimises the LPSP, LCOE and dumped power have been found after 150 generations of the GA optimisation procedure. Fig. 15 presents the Pareto optimal solutions obtained from the multi-objective optimisation of the HRES for the LF system case with ST + ORC back-up. The conflicting nature of the multi-objective problem is evidenced by the degree of scatter in the Pareto front. This is even clearer in the functional relationship

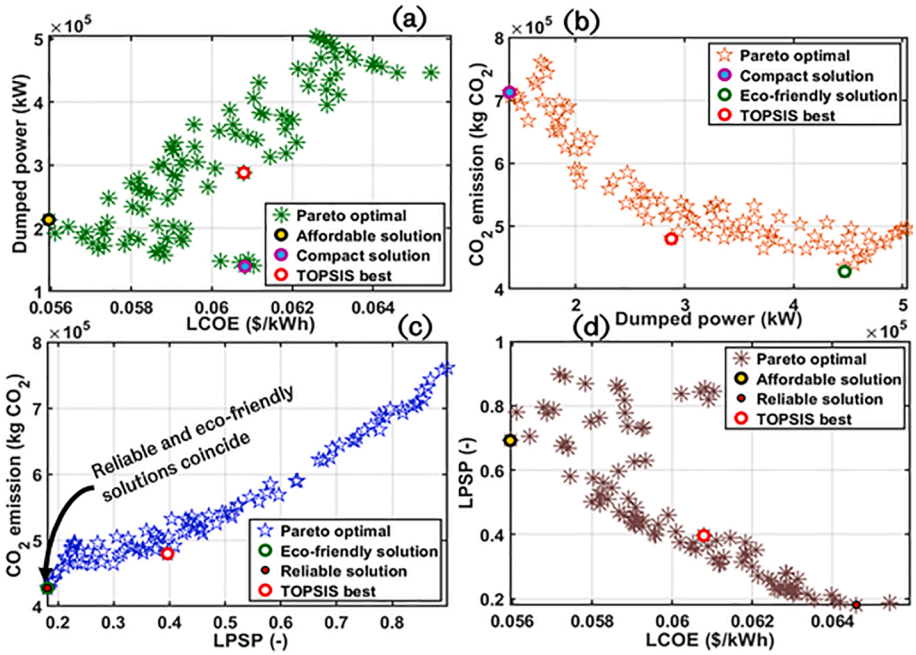

Fig. 15. Pareto front of the optimal system configuration found from the multi-objective optimisation for the load following with ST + ORC back-up case.

demonstrated by the objective functions presented in Fig. 15.

As Fig. 15 (a) shows, the LCOE and dumped power noticeably exhibit a positive relationship, since an increase in the size of the system will raise the energy cost and contribute to the increase in the dumped power. On the other hand, the dumped power and the CO_2 emitted from the energy system conflict as observed in Fig. 15 (b), because high penetration of green energy generators that are periodic and anti-correlated with the load demand, reduces the carbon emissions but increases the dumped power. For a similar reason, the LPSP is consistent with the CO_2 emissions as it is evident in Fig. 15 (c). While the LCOE exhibits an indirect relationship with the LPSP, i.e., increasing system reliability increases energy cost (Fig. 15 (d)).

Further, the ideal solutions from the perspective of reliability, eco-friendliness, compactness and affordability have been marked in Fig. 15 and it is evident that no solution simultaneously meets the ideal conditions from these standpoints. Hence, TOPSIS decision making tool has been deployed to obtain the best system configuration from the Pareto set in each case as highlighted in Fig. 15. The TOPSIS best in Fig. 15 (a) indicates the cheapest solution but is tangential to the indicated positive ideal solution from the perspective of dumped power. Similarly, in Fig. 15 (b), the TOPSIS best prioritizes reducing carbon emissions over dumped power and indicates a solution that is in close proximity to the positive ideal solution for carbon emissions minimisation. Regarding LPSP and CO_2 emissions, as it is evident in Fig. 15 (c), the TOPSIS best ensured comparable trade-off in these two objectives, while the LCOE is slightly prioritised more than the reliability (LPSP) in Fig. 15 (d). The priorities demonstrated in selecting the TOPSIS best reflect the weight assigned to each of these objectives in the selection process. It is clear that the reduction in the energy cost has been given the top priority, while reliability and sustainability are rated second and over the size.

Similar steps have been replicated to obtain the best system configuration in each of the examined system cases. The next section presents the comparison of the optimal system configurations obtained from the different cases to the base case (DG back-up HRES) from technical, economic and environmental perspectives. These HRES cases have been primarily formulated to evaluate the performance of different possible system configurations and compare results to the base case.

Table 6
Optimal system configuration in load following for all the examined cases.

Objective function	Case 1	Case 2	Base case
LCOE (cent/kWh)	7.72	6.08	15.58
LPSP (-)	0.3507	0.3962	0.3527
Dumped power (MWh)	309.7	287.8	305.9
CO_2 emissions (kg CO_2)	8.342×10^5	4.795×10^5	7.232×10^5
Number of PV	4×983	4×935	4×977
Wind Turbine type	EWT 52–250	EWT 52–250	EWT 52–250
Number of WT	5	5	5
Battery Type	Type 3	Type 2	Type 3
Number of batteries	4×30	4×26	4×30
Capacity of back-up engine (kW)	190	193	182.12
Annual PV Power (MWh)	724.25	688.16	719.84
Annual WT power (MWh)	330.26	330.26	330.26
Annual back-up power (MWh)	347.59	361.71	345.30

5.3.1. *Optimal system configurations in load following*

Two hybrid system configuration cases that utilise the load following (LF) dispatch strategy have been proposed in this study. Table 6 presents the optimal system configuration obtained for these cases and for the base case, while Fig. 16 presents the comparative analysis of the normalised results of the optimal system performance.

(i) Case 1: Hybrid WT-PV-BSS with ST back-up

This hybrid system case deploys sole Stirling engine to follow the positive net load in the system, when the renewable generators are unable to match the consumer's energy demand. Unlike in the base case where the DG is deployed for a similar purpose, the obtained optimal configuration in case 1 utilises slightly more PV generators (983 PV panels in parallel) as seen in Table 6. Therefore, the total power generated from the renewable generators increased marginally by 0.42% compared to the base case; hence, the slight increase in the dumped power by 2 MWh in case 1, since the both cases deployed equal amount of BSS to store the excess power. Correspondingly, the LPSP in case 1 (LPSP of 0.3501) is better than in the base case (LPSP of 0.3962), because the former utilised more PV generators (see, Fig. 16. Thus, the optimum configuration in case 1 is more reliable compared to the base case. On the other hand, LCOE of 7.72 cents/kWh is obtained in case 1, which represents a decrease of 50.45% compared to the base case (LCOE of 15.58 cents/kWh). This decrease is attributable to the lower unit cost

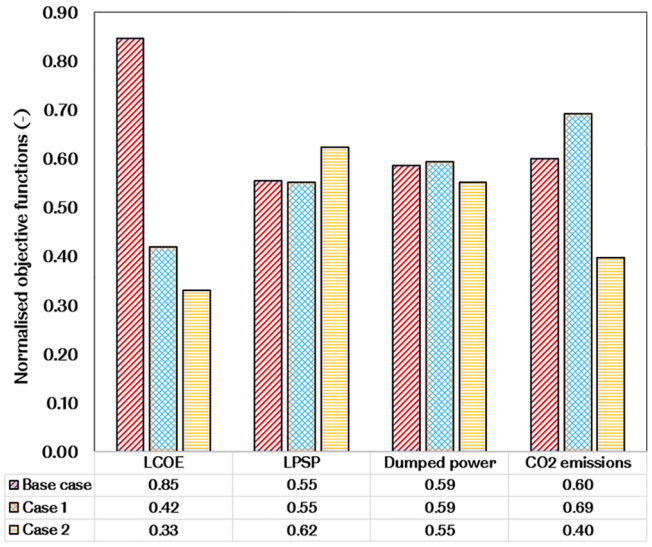

Fig. 16. Comparison of the results obtained from the optimal system configuration of the various system cases in load following for the normalised objective functions.

of fuel, cost of maintenance, capital cost, and even replacement cost associated with the deployment of the biomass fired ST back-up compared with the DG back-up. However, slight increase in the carbon emissions of 2.12% is notable in case 1 compared with the base case, due to the marginal increase in the utilisation of the ST back-up in the former compared to the latter as can be seen in Table 6.

(ii) Case 2: Hybrid WT-PV-BSS with ST + ORC back-up

This case proposes the deployment of combined ST + ORC to serve as the back-up to the HRES and augment its reliability. As it is evident in Table 6, the optimal system in case 2 employs fewer number of PV modules (935 PV panels in parallel) and BSS (26 type 2 BSS in parallel) with slightly higher capacity of ST + ORC back-up, to match the load. Consequently, the renewable generators produce 3.01% and 3.42% less power compared with the base case and case 1, respectively, and this reduces the dumped power by 18.1 MWh and 21.9 MWh in case 2 compared to the base case and case 1, respectively. As a result of the reduction in the deployment of renewable generators in the optimal configuration in this case, the system relies more on the ST + ORC back-up and this is evidenced by the slightly higher LPSP of 0.3962 compared to the base case (LPSP of 0.3527) and case 1 (LPSP of 0.3507) recorded in Fig. 16.

Interestingly, the high LPSP evident in case 2, which also implies the increased deployment of the ST + ORC back-up, did not generate an increase in the energy cost or emissions. This is because, the ORC utilises the recovered waste heat from the ST cooler to produce additional power; consequently, less fuel is consumed by the back-up to fulfill the net load. Moreover, unlike in case 1, the ST + ORC back-up operates at a higher efficiency, which implies more useful work is produced with less fuel. So, an energy cost of 6.08 cents/kWh is obtained and this is 60.79% lower than the base case but represents 21.14% reduction in LCOE compared with the sole ST back-up case. Similarly, the optimal configuration that deploys ST + ORC back-up reduces emissions by 33.70% (4.795×10^5 kg of CO_2) compared to the base case (7.232×10^5 kg of CO_2) and 42.52% compared to case 1 (8.342×10^5 kg of CO_2), because of the reduced consumption of woodchips fuel and higher efficiency of the heat engine.

Finally, from these results, it is evident that the optimal system configuration in case 3 that deploys combined ST + ORC back-up to follow the unmet load, offers reduced emissions, and cheaper energy due to the reduced fuel consumption, and a compact system size indicated by the lower dumped power. However, it relies more on the ST + ORC back-up because of the higher system efficiency of the combined power configuration.

Table 7
Optimal system configuration in circuit charging for all the examined back-up cases.

Objective function	Base case	Case 1	Case 2	Case 3
LCOE (cent/kWh)	15.89	8.13	7.88	15.91
LPSP (-)	0.3513	0.3677	0.3447	0.3796
Dumped power (MWh)	326.3	351.5	333.6	343.6
CO_2 emissions (kg CO_2)	7.53×10^5	7.42×10^5	9.21×10^5	7.53×10^5
Number of PV	4×993	4×999	4×1007	4×1009
Wind Turbine type	EWT 52–250	EWT 52–250	EWT 52–250	EWT 52–250
Number of WT	5	5	5	5
Battery Type	Type 3	Type 3	Type 3	Type 3
Number of batteries	4×30	4×30	4×30	4×29
Capacity of back-up (kW)	180	185	182	187
Annual PV Power (MWh)	731.62	736.05	741.94	743.09
Annual WT power (MWh)	330.25	330.25	330.25	330.25
Annual back-up power (MWh)	386.40	360.00	383.77	360.14

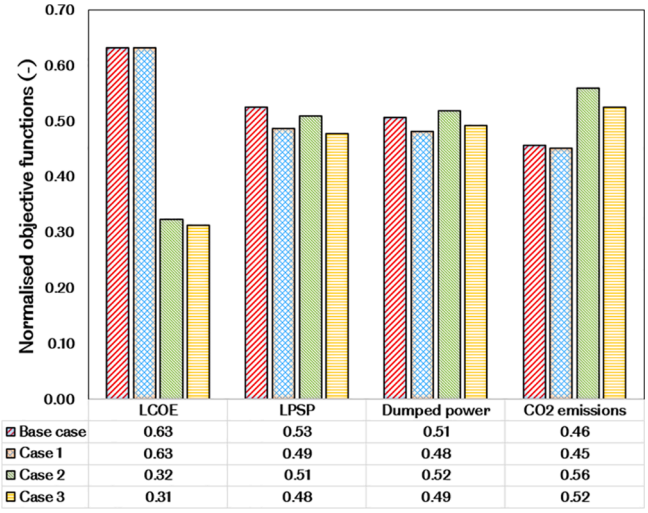

Fig. 17. Comparison of the results of the normalised objective functions obtained from the optimal system configuration of the various HRES cases in circuit charging.

5.3.2. Optimal system configurations in circuit charging

For the circuit charging dispatch strategy, five different system configurations have been formulated. The optimal system configuration obtained in these cases have been presented in Table 7, while Fig. 17 presents the comparison of the normalised results of the optimal system performance.

(i) Case 1: Hybrid WT-PV-BSS with 4-split DG back-up

Here, four-split DG have been deployed to fulfill the load when the renewable generators are unable to match the energy demand. The split DG will also charge the BSS while supplying the deficit power. The optimal system configuration obtained in this case has similar number of components as in the base case with the exception of six additional PV panels in parallel deployed to fulfill the energy demand more than in the base case. On the other hand, case 1 generates far less power from the DG back-up and this reduces the dumped power by 5% compared with the base case [19]. Similarly, the optimal system in this case has higher renewable fraction as indicated by the considerable lower LPSP of 0.3513 compared to the LPSP of 0.3796 obtained for the base case as

seen in Fig. 17. With the deployment of split DG, the commitment of the back-up to fulfilling the positive net load in the system is minimised; hence, the observed reduction in the dumped power and LPSP. Notwithstanding the remarkable reductions in the power dispatched from the DG back-up in this case, the LCOE of the optimal system did not change significantly compared to the base case, because of the higher number of PV generators deployed. Finally, the deployment of 4-split DG in this case minimises the carbon emissions of the one big DG case marginally by 1.41%, as can be seen in Fig. 17 where a slight drop in the normalised carbon emissions is evident.

(ii) Case 2: Hybrid WT-PV-BSS with one big ST back-up

This hybrid system configuration proposes the utilisation of one big ST back-up to augment the system reliability and charge the batteries. As Table 7 shows, the optimal configuration in case 2 has similar configuration as in the base case; however, it deploys more PV generators and produces 10.32 MWh more power from the renewable generators than the latter. On the contrary, it generates slightly less power from the ST back-up and correspondingly, yields lower LPSP of 0.3611 but with higher dumped power of 351.50 MWh compared to the base case (LPSP of 0.3796 and dumped power of 343.60 MWh). Further, the deployment of ST back-up to augment the reliability of the hybrid system minimises the energy cost by 48.9 % (LCOE of 8.13 cent/kWh) compared with the base case (LCOE of 15.91 cent/kWh), due to the higher cost of maintenance, replacement cost of DG and fuel cost (see, Fig. 17. Unfortunately, the carbon emissions increased by 22.38 % with this HRES arrangement compared to the base case, because of the low electrical efficiency of the heat engine ($\eta_{ST} = 0.21$). Finally, compared to case 1, this system case only offers an advantage in the form of reduced energy cost but dumps more power and has lower reliability and higher emissions than the former.

Case 3: Hybrid WT-PV-BSS with 4-split ST back-up

In this HRES configuration, four-split STs are deployed to fulfil the net load while simultaneously charging the batteries. It is seen in Table 7 that, the optimal configuration deploys more PV generators and slightly higher BSS compared to the base case and generates 11.47 MWh more power from the renewable generators. Consequently, it is 9.19% more reliant on renewable generators as represented by the lower LPSP of 0.3447 compared to 0.3796 for the base case. The notable power reductions in the deployment of 4-split STs back-up compared to one big ST (or DG) seen in Fig. 18 is another evidence of the high system reliability. Therefore, the dumped power is lower (10 MWh less) in this case compared to the base case. Also, the reduction in the commitment of the ST back-up to fulfilling the load with the utilisation of 4-split STs, the lower maintenance cost and fuel cost culminate in 50.5% decline in the LCOE in this case (LCOE of 7.88 cent/kWh) compared to the base case (LCOE of 15.91 cent/kWh). Nonetheless, the optimal configuration in case 3 emits 14.5% more CO_2 than in the base case, due to the low electrical efficiency of the ST although not as significant as in case 2, because of the reduction in the woodchips consumption with the utilisation of split STs. Finally, case 3 offers lower LCOE and LPSP but higher emissions and dumped power compared to case 1, while it performs better than the one big ST case in all indices (see also, Fig. 17).

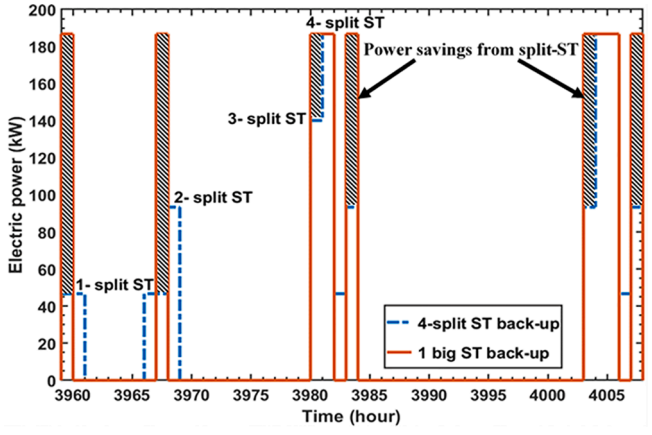

Fig. 18. Comparing hourly power dispatch from one big ST and 4-split STs.

5.3.3. Impact of deploying ST + ORC on optimal system in circuit charging

Two additional hybrid system configurations have been proposed to evaluate the optimal system performance when ST + ORC is deployed in circuit charging dispatch mode. The optimal configurations from these cases are presented in Table 8, while the performance indicators are presented in Fig. 19 and have been compared to the previous cases.

Case 4: Hybrid WT-PV-BSS with ST + ORC back-up

This configuration utilises ST + ORC as the back-up to the HRES while operating at the rated capacity of the topping cycle and also charging the BSS with the excess power generated. It is seen in Table 8 that the optimal system configuration obtained in this case utilises fewer number of PV generators but generates more power from the combined cycle back-up compared to cases 2 and 3. Consequently, the HRES in this case depends more on the back-up to fulfil the load demand and that is evidenced by the higher LPSP of 0.3801 compared to 0.3677 and 0.3447 for cases 2 and 3, respectively (see also, Fig. 19. Also, the dumped power in this optimal configuration is less than in case 2 but higher than case 3 that deploys 4-split STs. In spite of some of these observed unfavourable performance data, the utilisation of combined ST + ORC back-up in case 4 reduces the LCOE and CO_2 emissions by 22.26% and 44.25% and 19.79% and 40.53%, respectively compared with cases 2 and 3, respectively. This is a result of the higher efficiency of the ST + ORC back-up and the reduction in the fuel consumption compared to ST only. In contrast to the base case (one big DG back-up), the optimal system in this case offers 60.27% and 31.7% (slightly higher for case 3) lower LCOE and CO_2 emissions, respectively.

Case 5: Hybrid WT-PV-BSS with 4-split ST + ORC back-up

Case 5 deploys 4 small STs operating at their rated capacities as the back-up to the HRES with ORC bottoming cycle and will charge the batteries if generating excess power. As Table 8 reveals, the optimal configuration in this case is characterised by fewer PV generators (965 PV panels in parallel), reduced battery capacity (29 type 2 batteries in parallel) and lower or comparable back-up power compared to the other cases. Consequently, it has high LPSP (LPSP of 0.3929), i.e., increased reliance on biomass powered back-up generators but reduced dumped power compared to the other cases. In terms of energy cost and emissions, this HRES case reduces energy cost by 22.08%, 24.47% and 61.4% and emits less carbon (5.0429×10^5 kg of CO_2), which is evidenced by reductions in emissions of 41.65%, 45.25% and 33% than that of case 3,

Table 8
Optimal system configuration in circuit charging for all the examined back-up cases.

Objective function	Case 2	Case 3	Case 4	Case 5
LCOE (cent/kWh)	8.13	7.88	6.32	6.14
LPSP (-)	0.3677	0.3747	0.3801	0.3929
Dumped power (MWh)	351.5	333.6	337.3	320.0
CO_2 emissions (kg CO_2)	9.21×10^5	8.64×10^5	5.14×10^5	5.04×10^5
Number of PV	4×1007	4×1009	4×995	4×965
Wind Turbine type	EWT 52–250	EWT 52–250	EWT 52–250	EWT 52–250
Number of WT	5	5	5	5
Battery Type	Type 3	Type 3	Type 3	Type 2
Number of batteries	4×30	4×29	4×30	4×29
Capacity of back-up (kW)	182	187	180	190
Annual PV power (MWh)	741.94	743.09	733.10	711.00
Annual WT power (MWh)	330.25	330.25	330.25	330.25
Annual back-up power (MWh)	383.77	360.14	387.50	361.52

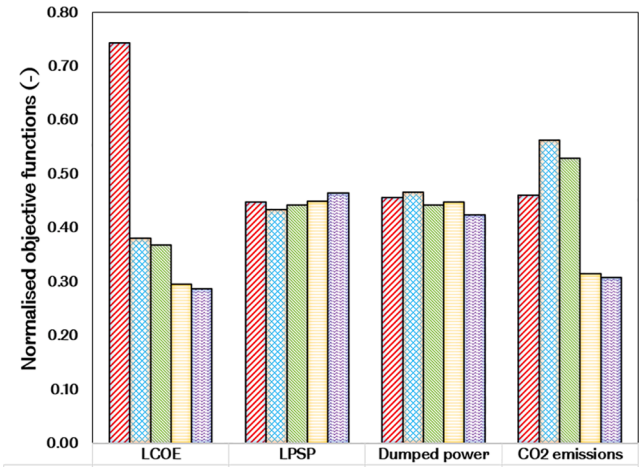

	LCOE	LPSP	Dumped power	CO2 emissions
Base case	0.74	0.45	0.46	0.46
Case 2	0.38	0.43	0.47	0.56
Case 3	0.37	0.44	0.44	0.53
Case 4	0.30	0.45	0.45	0.31
Case 5	0.29	0.46	0.42	0.31

Fig. 19. Comparison of the results of the normalised objective functions obtained from the optimal system configuration of the different HRES cases with ST back-up in circuit charging.

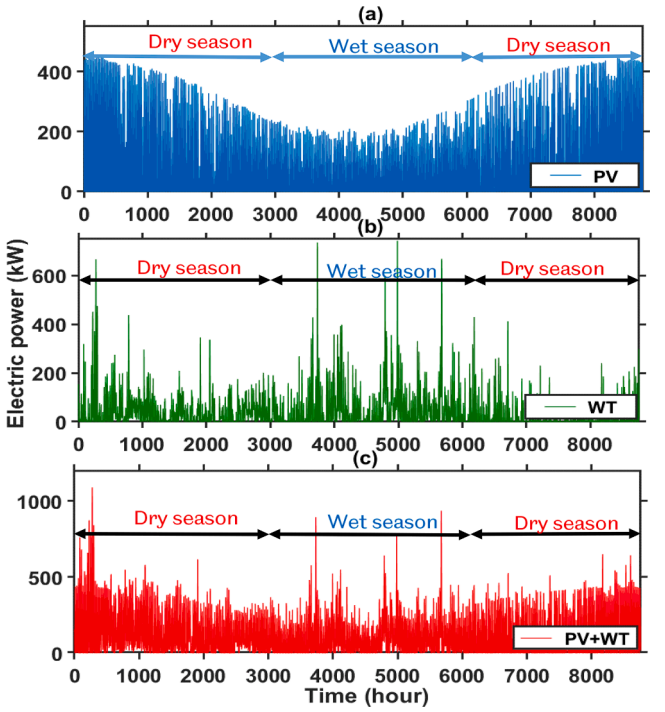

Fig. 20. Hourly generated power from the renewable generators in the optimal HRES configuration.

case 2 and the base case, respectively, but marginally lower than case 4 (See, Fig. 19). This can be attributed to the reduction in the commitment of the back-up to fulfilling the load demand, with the deployment of 4-split STs, on one hand and on the other hand, the utilisation of combined power configuration that minimises the fuel consumption of the ST + ORC back-up, by recovering the waste heat from the topping cycle.

It is clear from the presented results that the deployment of 4-split STs improve the performance of the HRES compared to the base case [19]. Further improvements in system performance indicators are notable with the deployment of ST + ORC back-up and split STs in CC. Nevertheless, the deployment of ST + ORC back-up in LF offers the best performance indicators. This solution is therefore, adopted for the simulation and sensitivity analysis undertaken in the subsequent sections.

5.4. Optimal HRES configuration simulation results

This section presents the results of the dynamic simulation of the best optimal configuration that gave the least LCOE, LPSP, CO_2 emissions and dumped power for the test location. As has been previously stated, the HRES configuration in case 3 that deploys combined ST + ORC back-up to augment the system reliability in the LF mode offers the best performance indicators. Consequently, the hourly electricity generation from the system units to fulfil the electric load of the customers in the two main seasonal conditions experienced annually in the test location; the dry and wet seasons [18] has been evaluated.

Fig. 20 represents the hourly power generation from the renewable generators in the test location for the best optimal system configuration. It is evident from Fig. 20 (a), that the power generation from the PV generator is strongly affected by the seasonal changes and drops from a peak generation of 450 kW at the beginning of the year (dry season) to a low value of 200 kW at the mid-year period (wet season). On the contrary, the power generation from the WT generator, Fig. 19 (b) is stochastic and records a few high spikes of over 600 kW, especially in the mid-year period (wet season). It is also noticeable in Fig. 19 (c) that the combined generation from the renewable generators increased remarkably with the hybridisation of the WT and PV. This results in the minimisation of the low power generation in the wet season from the PV generator as well as the many high power spikes from the WT generator. The observed trend highlights the complementarity of wind and PV and supports their hybridisation.

Further results of the dynamic performance of the best optimum HRES configuration, for two consecutive days in the (a) dry season and (b) wet season have been presented to gain additional insight into the impact of the seasonal variations on the optimal system performance. In Fig. 21, the dynamic simulation of the optimal system configuration in the test location has been presented for two-consecutive days in the dry season (Fig. 21 (a)) and wet season (Fig. 21 (b)).

As Fig. 21 (a) depicts, due to the clear weather that characterises the dry season, more power is generated by the solar PV and WT; hence, the high excess power in the dry season compared to the wet season. Correspondingly, the battery is deployed more in the dry season to supply the unmet load as evidenced by the several cycles of charging and discharging of the battery in Fig. 21 (a) and Fig. 22. On the other hand, the ST + ORC back-up follows the load only a few times in the dry season, which helps to minimise its contribution to fulfilling the load. Unlike in the dry season, the wet season is marked with high deployment of the ST + ORC back-up to augment the reliability of the HRES, due to the low power generation from the green generators. Consequently, there is insufficient excess power to charge the batteries, which is responsible for the few cycles of charging and discharging of the battery noticeable in Fig. 21 (b) and Fig. 22, in the wet season. So, the battery remains in its minimum SOC most of the time in this season, and this regrettably may affect the life of this component [15].

Therefore, because batteries are utilised more in the dry season compared with the ST + ORC back-up, the energy cost is lower in the dry season than in the wet season. Nonetheless, high dumped power is evident in the dry season as can be seen in Fig. 23 compared to the wet season, because of the higher power generation from the non-programmable generators. Further, there may be challenges with the availability of the biomass fuel in the wet season, considering that the system is designed for use in a remote location, where the common practice is to deploy the traditional open solar drying to regulate the moisture content of the woodchips. To solve this problem, in-situ drying of the woodchips fuel has been proposed [29], whereby the waste flue gas will be deployed to dry the woodchips in the wet season. Thus the

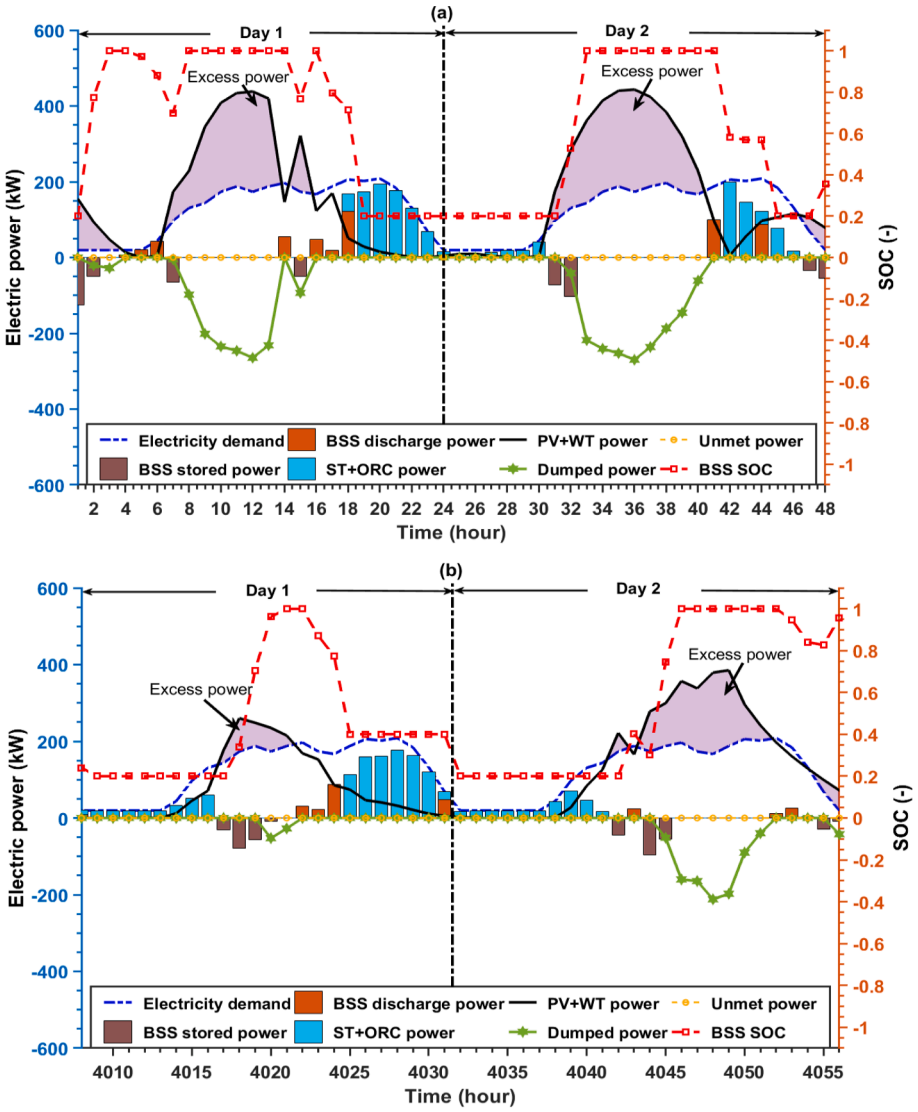

Fig. 21. Dynamic simulation of the optimal system configuration for two consecutive days in the design location in (a) dry season and (b) wet season.

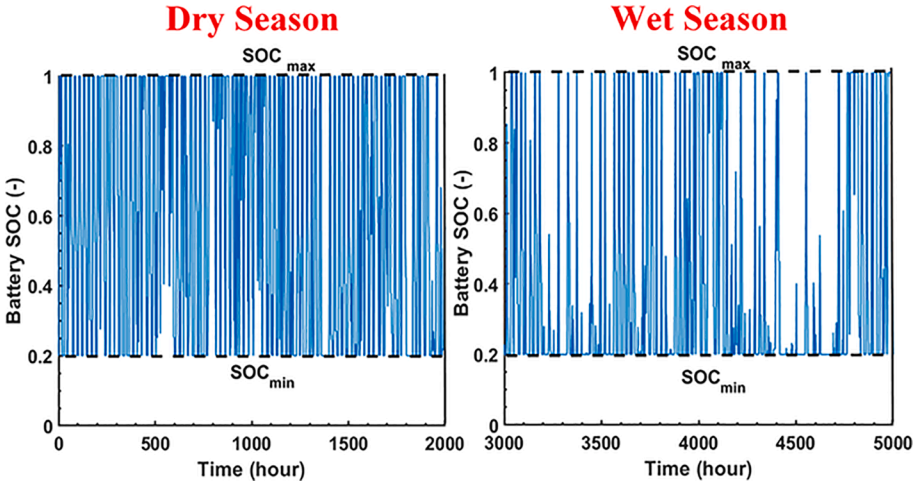

Fig. 22. Battery state of charge in the dry and wet seasons when deployed to argument system reliability in the test location.

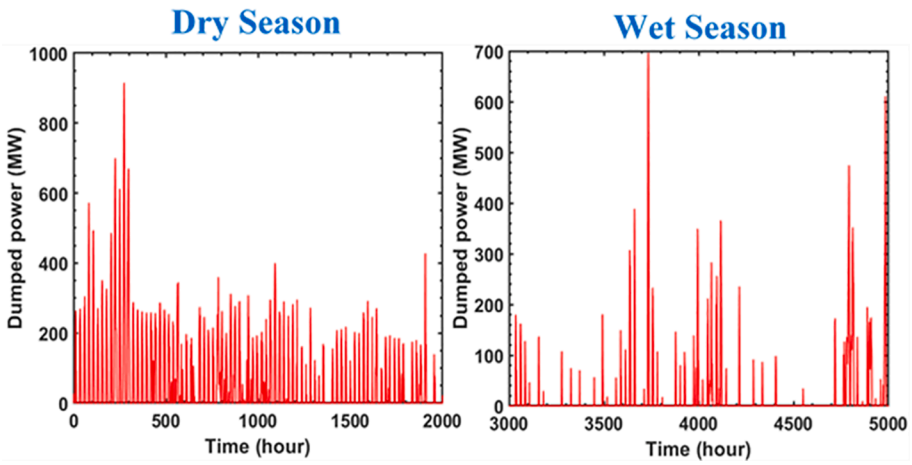

Fig. 23. Dumped power from the energy system when deployed to meet the electric load in the test load in the dry and wet seasons.

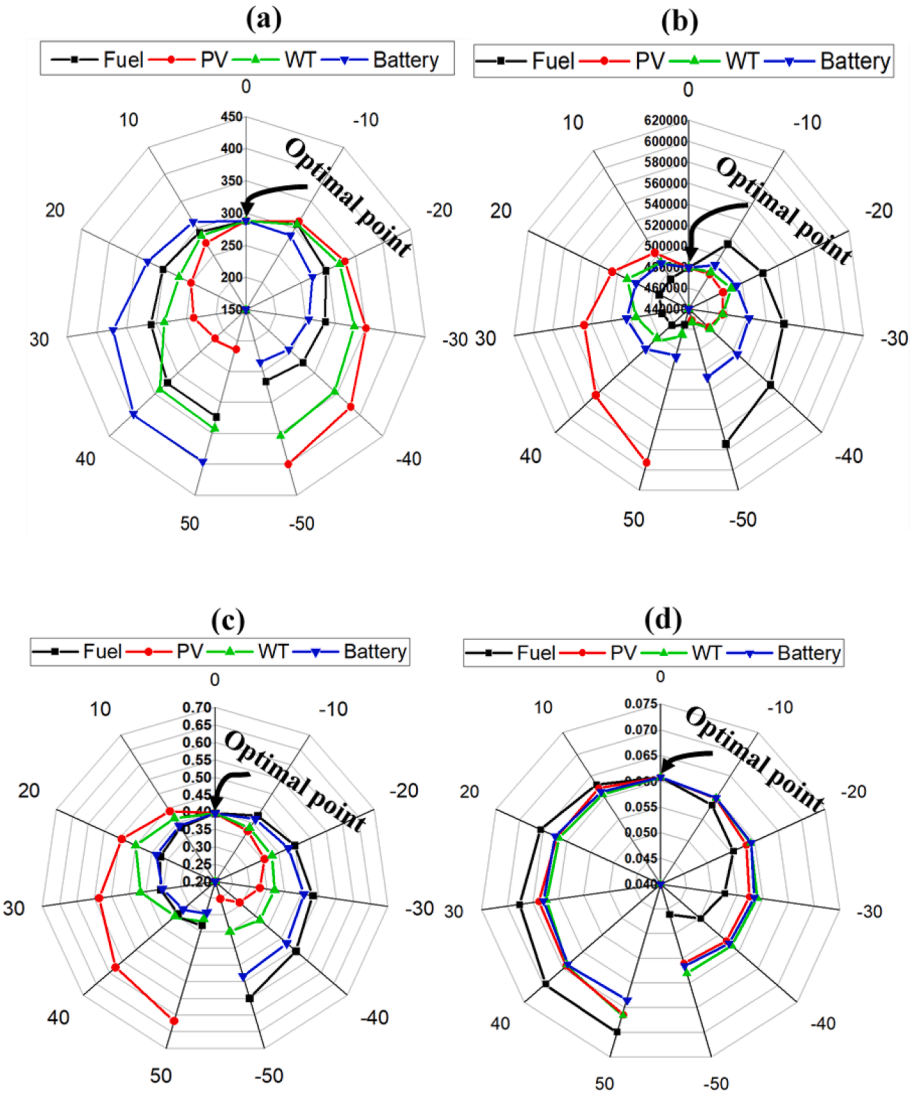

Fig. 24. Impact of changes in component and fuel price on the (a) dumped power (MWh), (b) carbon emissions (kg CO_2), (c) LPSP (–) and (d) LCOE (cent/kWh) of the best optimal configuration.

quality of the woodchips fuel is regulated and its availability is guaranteed all year round.

5.5. Sensitivity analysis

To investigate the effect of variation in the market price and size of key system components and other parameters on the performance of the optimal configuration, sensitivity analysis has been performed on the optimal system. For the sensitivity analysis on the impact of market price changes on the optimal HRES, each of the unit prices of the PV panel, wind turbine, woodchips fuel and battery has been varied between −50% to +50% with a step increase of 10% while keeping the others constant. Then, the GA optimiser and TOPSIS were deployed for each step size, to find the optimum system configuration as well as obtain the corresponding LPSP, LCOE, dumped power and CO_2 emissions. On the other hand, the quantity (size) of one of the key system components (PV panel, WT, batteries and ST + ORC) in the optimal system configuration has been altered by −50% to +50% with a step increase of 5%, while the others were fixed. Then, the optimum configuration is simulated and consequently, the LPSP, LCOE, dumped power and CO_2 emissions for each step increase is obtained. Fig. 24 and Fig. 25 present the results of the sensitivity analysis carried out on the optimal system configuration on a radar chart.

Fig. 24 (a), (b), (c) and (d) show the impact of the variations in the market price of the PV, WT, BSS and woodchips fuel on the dumped power, CO_2 emissions, LPSP and LCOE, respectively, of the best optimal system configuration; load following dispatch mode with combined ST + ORC back-up (case 3). As it is evident in Fig. 24 (a), the increase in the cost of the PV generators catalyses a decrease in the dumped power by as high as 28% for 150% increase in price, because fewer components are deployed. Consequently, the system emits more carbon pollutants (see, Fig. 23 (b)) and also becomes less reliable as evidenced by the high LPSP (more than 50% change) in Fig. 24 (c). This also confirms the indicated positive relationship between reliability and eco-friendliness in the Pareto front in Fig. 15. Meanwhile, the LCOE of the system increases marginally as the PV price increases and about 8.33% rise in LCOE is observed for a 150% hike in the component's price as seen in Fig. 24 (d). An opposite effect is noticeable with the decrease in the cost of the component although, it is less evident for all other objective functions with the exception of the dumped power.

Contrarily, an increase in the price of the WT generates a dramatic effect on the objective functions. The CO_2 emissions and LPSP increase slightly before decreasing marginally (about 13% decline in the LPSP for 150% price change) as noticeable in Fig. 24 (b) and (c), respectively. This dramatic trend is driven by the fact that with further increase in the cost of the WT, the system opts for cheaper PV generators to replace the

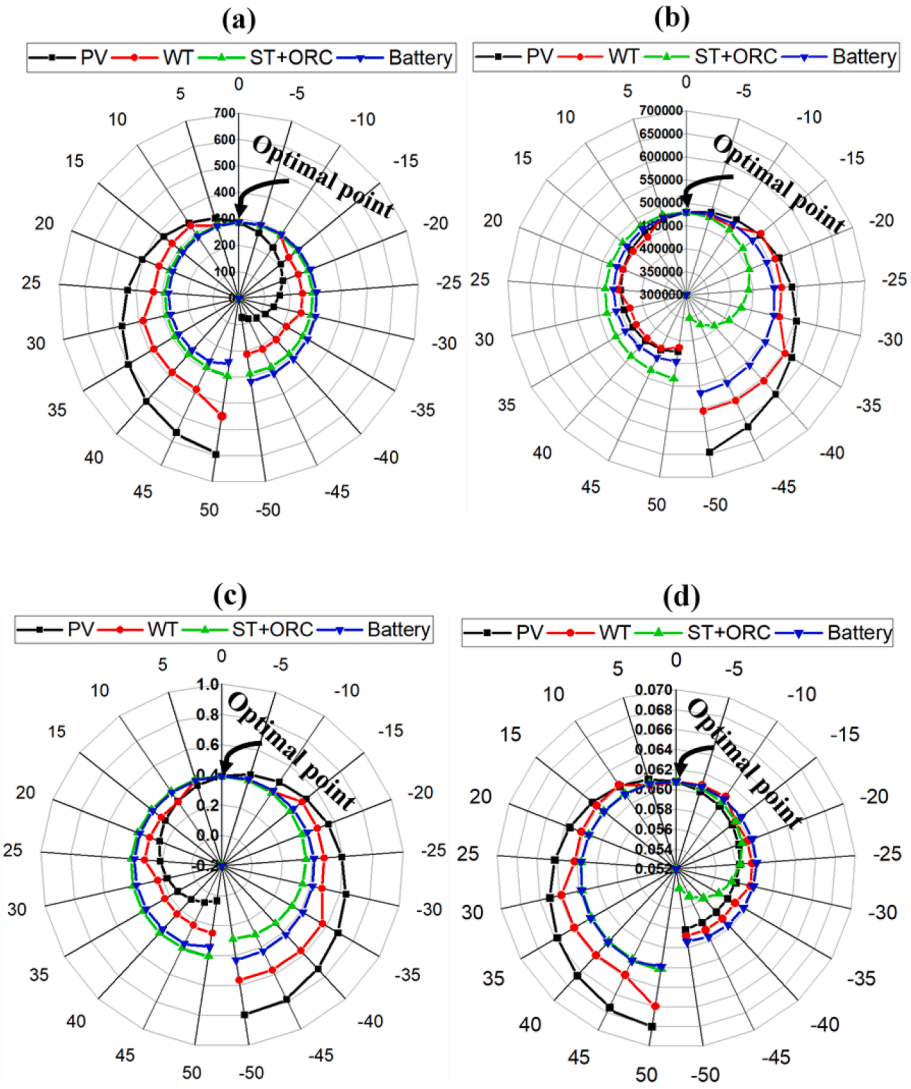

Fig. 25. Impact of changes in component size on the (a) dumped power (MWh) (b) carbon emissions (kg CO_2) (c) LPSP (–) and (d) LCOE (cent/kWh) of the best optimal configuration in load following.

former resulting in the observed decline. Consequently, the dumped power initially decreases with the increase in the price of the green generator, but increases substantially as more PV generators are deployed with the increase in price and contributed about 25% increase with 150% rise in component's price as seen in Fig. 24 (a). On the other hand, as the price of the WT increases, the LCOE increases substantially by the same magnitude as in the PV (see, Fig. 24 (d)). However, the decrease in the price of this non-programmable generator produces similar and comparable effect as the decrease in the price of the PV generator. A decrease in the price of the WT induces a decrease in all the objective functions except the dumped power that notably increases because more clean generators are deployed.

The increase in the price of the batteries, significantly increases the dumped power as expected by about 30% for a 150% change in component's price (see, Fig. 24 (a)), due to the corresponding reduction in the storage capacity. Hence, more green generators are included in the optimal system to augment the apparent shortfall in the storage capacity of the batteries. Consequently, the carbon emissions and LPSP that are complementary (see, Fig. 15 evidently reduce albeit marginally, with the increase in the price of the batteries (see, Fig. 24 (b) and (c)). However, as can be observed, the LCOE increases significantly with the increase in the price of this component (Fig. 24 (d)). The opposite trend is evidenced as the price of the batteries fall and the most significant change can be observed in the LPSP.

Similarly, as the price of the woodchips fuel increases, the dumped power increases substantially by about 11% for 150% change in price (Fig. 24 (a)), while the energy cost rose by almost 15% for a similar price change (Fig. 24 (d)). This is expected because more green generators are deployed to reduce the impact of the high cost of the fuel. Hence, the CO_2 emissions and LPSP decrease with the increase in the cost of the fuel as it is evident in Fig. 24 (b) and (c). The opposite effect is noticeable with the reduction in the price of the woodchips fuel. Overall, the change in the price of the PV has the most impact on the optimal system's LPSP and CO_2 emissions, while the change in the price of the battery and woodchips fuel have the most impact on the dumped power and LCOE, respectively.

Fig. 25 presents the impact of the changes in the number of PV, WT, BSS and capacity of ST + ORC back-up on the dumped power, CO_2 emissions, LPSP and LCOE of the best optimal HRES configuration (Case 3 in load following mode). It is evident in Fig. 25 (a) that increasing the size of the renewable generators leads to an increase in the dumped power, while the dumped power decreases with a decrease in the number of these components. The renewable generators are non-programmable and periodic or stochastic in their power generation; hence, their hourly power generation anti-correlates with the load demand [53]. Correspondingly, the carbon emissions (Fig. 25 (b)) and LPSP (Fig. 25 (c)) decrease while the LCOE increases (Fig. 25 (d)) with the increase in the number of PV and WT. The opposite trend is indicated with the decrease in the number of these renewable generators.

On the contrary, as the number of batteries in the optimum system configuration increases, the dumped power reduces as evident in Fig. 25 (a), because more excess power is stored in the BSS, while the opposite effect is observed with a reduction in the number of this component in the optimum configuration. As a consequence, the carbon emissions reduce as seen in Fig. 25 (b), while the LPSP changes only marginally (Fig. 25 (c)), whereas the LCOE increases substantially with the increase in the number of the batteries (Fig. 25 (d)). The opposite trend is indicated with the reduction in the number of batteries.

Meanwhile, the variation in the capacity of the ST + ORC back-up did not impact the dumped power in the load following mode (Fig. 25 (a)) as could be imagined, because the back-up merely follows the load. However, the system emits more CO_2 and becomes less reliable as evidenced by the slight rise in the LPSP with the increase in the capacity of the ST + ORC back-up as represented in Fig. 25 (b) and (c), respectively. Similarly, the LCOE increases remarkably with the increase in the capacity of the engine. On the other hand, the LCOE and CO_2 emissions decrease significantly as the capacity of the back-up decreases, while marginal increase in the LPSP is observed.

Overall, the variation in the number of PV generators in the optimum system configuration altered the dumped power, LPSP and LCOE [9] more than any other component. The most significant change in the carbon emissions is observed with the variation in the number of PV and capacity of ST + ORC back-up in the optimum system configuration. While the change in the number of WT generator and ST + ORC back-up capacity have comparable impact on the system's energy cost. The variation in the number of batteries in the optimal system configuration affects the LCOE only marginally. Finally, the change in the number of PV generators that generates about 50% of the total power supplied to the electric load by the HRES, expectedly has the most impact on the optimal system's performance and this further highlights the significance of the PV generator in the optimal HRES configuration for this test location.

6. Conclusion and future work

This paper proposes the deployment of woodchips biomass powered combined ST + ORC and split ST back-ups to increase the reliability of a hybrid WT-PV-BSS when the system is in the load following (LF) and circuit charging (CC) dispatch modes, respectively. First, the optimal number and types of the system components that simultaneously minimises the levelised cost of energy (LCOE), loss of power supply probability (LPSP) and dumped power in each of the proposed HRES configurations were found by the deployment of the multi-objective genetic algorithm and the TOPSIS decision making tool. The LCOE, LPSP, dumped power and CO_2 emissions of the optimal HRES configuration have been compared to the base case; DG back-up system in both dispatch modes and other test cases formulated. Then, the hourly performance of the best system configuration was simulated for the two seasons that characterise the test location. Finally, the impact of the change in the market price and size of the system components and fuel on the performance of the optimum system configurations were investigated by means of a sensitivity analysis. The following vital conclusions can be drawn from the study:

Replacing DG with sole ST in LF dispatch mode reduces the optimal system energy cost by 50% compared to the base case. However, additional reductions in LCOE, CO_2 emissions and dumped power of 60.79%, 33.70% and 2.91%, respectively are evident with the deployment of combined ST + ORC back-up compared to the base case, although the optimal system slightly becomes more reliant on the ST + ORC back-up evidenced by a marginal increase in the LPSP.

While deploying four-split STs (4-split DG) in CC reduces the dumped power by 5.1% (5.03%) compared with the one big ST (DG) case. Higher reductions in dumped power by 8.96% is notable with the deployment of 4-split ST + ORC compared with one big ST case and by 6.89% compared with one big DG (base case). Other reductions in the LCOE, LPSP and CO_2 emissions of 61.4%, 33% and 24.5%, respectively are noticeable when 4-split ST + ORC is deployed as the HRES back-up in CC compared to the base case.

Seasonal variation in the test location affects the performance of the optimal system configuration. The energy cost is evidently low in the dry season marked by high generation from the green generators and increased power storage in the batteries and consequently, low deployment of the ST + ORC back-up although increased power dumping is also observed. Contrarily, the wet season is notable for high energy cost, because of the increased utilisation of the biomass back-up, as a result of low generation from the green generators.

The increase in the price of the battery and fuel reduces the carbon emissions and the LPSP but increases the dumped power, while the increase in the price of the WT more dramatically impacts the LPSP, carbon emissions and dumped power. The change in the price of the PV yields the opposite effect on the optimal HRES compared to the battery or fuel, with the exemption of the system LCOE, where increment in the

market price of any of the parameters produces corresponding increase and vice versa. The most variation in the system performance is observed with the change in the PV price.

Increment in the number of green generators in the optimal system increases the dumped power and energy cost but reduces the carbon emissions and improves the system's reliability and vice versa. The opposite trend is evidenced with the increase in the number of the battery storage and capacity of the ST + ORC back-up in the optimal HRES configuration. However, the inclusion of more PV generator or its reduction in the optimal HRES system configuration causes more variation in its performance.

This study has established the performance improvements of a hybrid system that deploys biomass powered 4-split STs or combined ST + ORC back-up to augment the system reliability in CC or LF dispatch strategies. It is clear from the presented results based on the data deployed for this study that the proposed back-ups for the HRES will offer lower energy cost, carbon emissions and dumped power, and improved system reliability compared to the traditional DG. Hence, it can be plausible replacements for the DG to augment the reliability of green energy based hybrid systems. Finally, it is evident that the dispatch strategy and split back-up have strong impact on the optimal number of components and performance of the hybrid system. Therefore, bi-level optimisation of the HRES will be conducted in a future work, to simultaneously optimise the configuration and the control strategy as well as investigate the wider impact of split back-up on the energy system's performance.

CRediT authorship contribution statement

Godfrey T. Udeh: Conceptualization, Investigation, Methodology, Software, Validation, Formal analysis, Writing – original draft. **Stavros Michailos:** Conceptualization, Methodology, Software, Validation, Writing – review & editing. **Derek Ingham:** Resources, Writing – review & editing, Project administration. **Kevin J. Hughes:** Resources, Writing – review & editing, Project administration. **Lin Ma:** Conceptualization, Writing – review & editing, Supervision, Project administration. **Mohammed Pourkashanian:** Resources, Writing – review & editing, Supervision, Project administration.

Declaration of Competing Interest

The authors declare that they have no known competing financial interests or personal relationships that could have appeared to influence the work reported in this paper.

Acknowledgements

This study was funded by the Petroleum Technology Development Fund, an agency of the Ministry of Petroleum Resources, in Nigeria.

Appendix A. Supplementary data

Supplementary data to this article can be found online at https://doi.org/10.1016/j.enconman.2022.115370.

References

[1] Bhargava SK, Das SS, Paliwal P. Multi-objective optimization for sizing of solar-wind based hybrid power system : a review 2014;3:195–201.
[2] AlBadwawi R, Abusara M, Mallick T. A review of hybrid solar PV and wind energy system. Smart Sci 2015;3:127–38. https://doi.org/10.6493/SmartSci.2015.324.
[3] Clarke DP, Al-Abdeli YM, Kothapalli G. Multi-objective optimisation of renewable hybrid energy systems with desalination. Energy 2015;88:457–68. https://doi.org/10.1016/j.energy.2015.05.065.
[4] Al Busaidi AS, Kazem HA, Al-Badi AH, Farooq KM. A review of optimum sizing of hybrid PV-wind renewable energy systems in oman. Renew Sustain Energy Rev 2016;53:185–93. https://doi.org/10.1016/j.rser.2015.08.039.
[5] Nagapurkar P, Smith JD. Techno-economic optimization and environmental Life Cycle Assessment (LCA) of microgrids located in the US using genetic algorithm. Energy Convers Manag 2019;181:272–91. https://doi.org/10.1016/j.enconman.2018.11.072.
[6] Bukar AL, Tan CW, Lau KY. Optimal sizing of an autonomous photovoltaic/wind/battery/diesel generator microgrid using grasshopper optimization algorithm. Sol Energy 2019;188:685–96. https://doi.org/10.1016/j.solener.2019.06.050.
[7] Tégani I, Aboubou A, Ayad MY, Becherif M, Saadi R, Kraa O. Optimal sizing design and energy management of stand-alone photovoltaic/wind generator systems. Energy Procedia 2014;50:163–70. https://doi.org/10.1016/j.egypro.2014.06.020.
[8] Cristóbal-Monreal IR, Dufo-López R. Optimisation of photovoltaic-diesel-battery stand-alone systems minimising system weight. Energy Convers Manag 2016;119:279–88. https://doi.org/10.1016/j.enconman.2016.04.050.
[9] Ramli MAM, Bouchekara HREH, Alghamdi AS. Optimal sizing of PV/wind/diesel hybrid microgrid system using multi-objective self-adaptive differential evolution algorithm. Renew Energy 2018;121:400–11. https://doi.org/10.1016/j.renene.2018.01.058.
[10] Wu J, Tan Z, Wang K, Liang Yi, Zhou J. Research on multi-objective optimization model for hybrid energy system considering combination of wind power and energy storage. Sustain 2021;13(6):3098. https://doi.org/10.3390/su13063098.
[11] Barakat S, Ibrahim H, Elbaset AA. Multi-objective optimization of grid-connected PV-wind hybrid system considering reliability, cost, and environmental aspects. Sustain Cities Soc 2020;60:102178. https://doi.org/10.1016/j.scs.2020.102178.
[12] Zhao J, Yuan X. Multi-objective optimization of stand-alone hybrid PV-wind-diesel-battery system using improved fruit fly optimization algorithm. Soft Comput 2016;20(7):2841–53. https://doi.org/10.1007/s00500-015-1685-6.
[13] Moradi H, Esfahanian M, Abtahi A, Zilouchian A. Optimization and energy management of a standalone hybrid microgrid in the presence of battery storage system. Energy 2018;147:226–38. https://doi.org/10.1016/j.energy.2018.01.016.
[14] Rathish RJ, Mahadevan K, Selvaraj SK, Booma J. Multi-objective evolutionary optimization with genetic algorithm for the design of off-grid PV-wind-battery-diesel system. Soft Comput 2021;25(4):3175–94. https://doi.org/10.1007/s00500-020-05372-y.
[15] Dufo-López R, Cristóbal-Monreal IR, Yusta JM. Optimisation of PV-wind-diesel-battery stand-alone systems to minimise cost and maximise human development index and job creation. Renew Energy 2016;94:280–93. https://doi.org/10.1016/j.renene.2016.03.065.
[16] Sadeghi D, Hesami Naghshbandy A, Bahramara S. Optimal sizing of hybrid renewable energy systems in presence of electric vehicles using multi-objective particle swarm optimization. Energy 2020;209:118471. https://doi.org/10.1016/j.energy.2020.118471.
[17] Xu X, Hu W, Cao D, Huang Q, Chen C, Chen Z. Optimized sizing of a standalone PV-wind-hydropower station with pumped-storage installation hybrid energy system. Renew Energy 2020;147:1418–31. https://doi.org/10.1016/j.renene.2019.09.099.
[18] Bukar AL, Tan CW, Yiew LK, Ayop R, Tan WS. A rule-based energy management scheme for long-term optimal capacity planning of grid-independent microgrid optimized by multi-objective grasshopper optimization algorithm. Energy Convers. Manag. 2020;221. doi:10.1016/j.enconman.2020.113161.
[19] Ogunjuyigbe ASO, Ayodele TR, Akinola OA. Optimal allocation and sizing of PV/Wind/Split-diesel/Battery hybrid energy system for minimizing life cycle cost, carbon emission and dump energy of remote residential building. Appl. Energy 2016;171:153–71. https://doi.org/10.1016/j.apenergy.2016.03.051.
[20] Gonzalez A, Riba J-R-R, Esteban B, Rius A. Environmental and cost optimal design of a biomass–Wind–PV electricity generation system. Renew. Energy 2018;126:420–30. https://doi.org/10.1016/J.RENENE.2018.03.062.
[21] Sawle Y, Gupta SC, Bohre AK. Optimal sizing of standalone PV/Wind/Biomass hybrid energy system using GA and PSO optimization technique. Energy Procedia 2017;117:690–8. https://doi.org/10.1016/j.egypro.2017.05.183.
[22] Maleki A, Rosen MA, Pourfayaz F. Optimal operation of a grid-connected hybrid renewable energy system for residential applications 2017. doi:10.3390/su9081314.
[23] Sigarchian SG, Paleta R, Malmquist A, Pina A. Feasibility study of using a biogas engine as backup in a decentralized hybrid (PV/wind/battery) power generation system – case study Kenya. Energy 2015;90:1830–41. https://doi.org/10.1016/j.energy.2015.07.008.
[24] Patel AM, Singal SK. Economic analysis of integrated renewable energy system for electrification of remote rural area having scattered population. Int J Renew Energy Res 2018;8:523–39.
[25] González-Pino I, Campos-Celador A, Pérez-Iribarren E, Terés-Zubiaga J, Sala JM. Parametric study of the operational and economic feasibility of Stirling micro-cogeneration devices in Spain. Appl Therm Eng 2014;71(2):821–9. https://doi.org/10.1016/j.applthermaleng.2013.12.020.
[26] Bocci E, Sisinni M, Moneti M, Vecchione L, Di Carlo A, Villarini M. State of art of small scale biomass gasification power systems: a review of the different typologies. Energy Procedia 2014;45:247–56. https://doi.org/10.1016/j.egypro.2014.01.027.
[27] Parente A, Galletti C, Riccardi J, Schiavetti M, Tognotti L. Experimental and numerical investigation of a micro-CHP flameless unit. Appl Energy 2012;89(1):203–14. https://doi.org/10.1016/j.apenergy.2011.06.055.
[28] Thiers S, Aoun B, Peuportier B. Experimental characterization, modeling and simulation of a wood pellet micro-combined heat and power unit used as a heat source for a residential building. Energy Build 2010;42(6):896–903. https://doi.org/10.1016/j.enbuild.2009.12.011.
[29] Udeh GT, Michailos S, Ingham D, Hughes KJ, Ma L, Pourkashanian M. A techno-enviro-economic assessment of a biomass fuelled micro-CCHP driven by a hybrid

Stirling and ORC engine. Energy Convers Manag 2021;227:113601. https://doi.org/10.1016/j.enconman.2020.113601.
[30] Dufo-López R, Bernal-Agustín JL, Yusta-Loyo JM, Domínguez-Navarro JA, Ramírez-Rosado IJ, Lujano J, et al. Multi-objective optimization minimizing cost and life cycle emissions of stand-alone PV-wind-diesel systems with batteries storage. Appl Energy 2011;88(11):4033–41. https://doi.org/10.1016/j.apenergy.2011.04.019.
[31] Models WT. Wind Turbines n.d. www.en.wind-turbine-models.com (accessed June 1, 2021).
[32] Bhandari B, Poudel SR, Lee K-T, Ahn S-H. Mathematical modeling of hybrid renewable energy system: a review on small hydro-solar-wind power generation. Int J Precis Eng Manuf Technol 2014;1(2):157–73. https://doi.org/10.1007/s40684-014-0021-4.
[33] Lujano-Rojas JM, Dufo-López R, Bernal-Agustín JL. Optimal sizing of small wind/battery systems considering the DC bus voltage stability effect on energy capture, wind speed variability, and load uncertainty. Appl Energy 2012;93:404–12. https://doi.org/10.1016/j.apenergy.2011.12.035.
[34] PV GIS. Satellite data n.d. https://ec.europa.eu/jrc/en/PVGIS/releases/pvgis51 (accessed January 8, 2021).
[35] Badea N. Design for micro-combined cooling, heating and power systems. Springer Berlin Heidelberg; 2015. doi:10.1007/978-1-4471-6254-4.
[36] Cozzolino R, Tribioli L, Bella G. Power management of a hybrid renewable system for artificial islands: a case study. Energy 2016;106:774–89. https://doi.org/10.1016/j.energy.2015.12.118.
[37] ICPC. ICPC report on emissions n.d. http://www.ipcc-nggip.iges.or.jp/public/2006gl/pdf/2_Volume2/V2_2_Ch2_Stationary_Combustion.pdf.
[38] HOPPECKE Sun Power n.d. https://voltaconsolar.com/batteries/agm-lead-acid/hoppecke-sun-power.html (accessed February 5, 2021).
[39] Solaris. Candian Solar Panel n.d. https://www.solaris-shop.com/canadian-solar-kumax-cs3u-340p-340w-poly-solar-panel/ (accessed March 6, 2021).
[40] Olatomiwa L, Mekhilef S, Ismail MS, Moghavvemi M. Energy management strategies in hybrid renewable energy systems: a review. Renew Sustain Energy Rev 2016;62:821–35. https://doi.org/10.1016/j.rser.2016.05.040.
[41] Lu J, Wang W, Zhang Y, Cheng S. Multi-objective optimal design of stand-alone hybrid energy system using entropy weight method based on HOMER. Energies 2017;10:1664. https://doi.org/10.3390/en10101664.
[42] National Renewable Energy Laboratory. U.S. Solar Photovoltaic System and Energy Storage Cost Benchmark: Q1 2020; 2021.
[43] Entezari A, Manizadeh A, Ahmadi R. Energetical, exergetical and economical optimization analysis of combined power generation system of gas turbine and Stirling engine. Energy Convers Manag 2018;159:189–203. https://doi.org/10.1016/j.enconman.2018.01.012.
[44] Quoilin S, Van Den BM, Declaye S, Dewallef P, Lemort V. Techno-economic survey of organic rankine cycle (ORC) systems. Renew Sustain Energy Rev 2013;22:168–86. https://doi.org/10.1016/j.rser.2013.01.028.
[45] Shayeghi H, Hashemi Y. Application of fuzzy decision-making based on INSGA-II to designing PV-wind hybrid system. Eng Appl Artif Intell 2015;45:1–17. https://doi.org/10.1016/j.engappai.2015.04.013.
[46] Azaza M, Wallin F. Multi objective particle swarm optimization of hybrid micro-grid system: a case study in Sweden. Energy 2017;123:108–18. https://doi.org/10.1016/j.energy.2017.01.149.
[47] Reddy MJ, Kumar DN. Multi-objective optimization using evolutionary algorithms. Water Resour Manag 2006;20:861–78.
[48] Kuo T. A modified TOPSIS with a different ranking index. Eur J Oper Res 2017;260(1):152–60. https://doi.org/10.1016/j.ejor.2016.11.052.
[49] Perera ATD, Attalage RA, Perera KKCK, Dassanayake VPC. A hybrid tool to combine multi-objective optimization and multi-criterion decision making in designing standalone hybrid energy systems. Appl Energy 2013;107:412–25. https://doi.org/10.1016/j.apenergy.2013.02.049.
[50] Nigerian Rural Electrification Agency. Nigeria minigrid investment brief 2017:25.
[51] Olatomiwa L, Mekhilef S, Huda ASN, Ohunakin OS. Economic evaluation of hybrid energy systems for rural electrification in six geo-political zones of Nigeria. Renew Energy 2015;83:435–46. https://doi.org/10.1016/j.renene.2015.04.057.
[52] Akinrinola FS. Torrefaction and combustion properties of some Nigerian biomass. University of Leeds; 2014.
[53] Park H, Baldick R. Integration of compressed air energy storage systems co-located with wind resources in the ERCOT transmission system. Int J Electr Power Energy Syst 2017;90:181–9. https://doi.org/10.1016/j.ijepes.2017.01.021.
[54] Saaty TL. A scaling method for priorities in hierarchical structures. J Math Psychol 1977;15(3):234–81. https://doi.org/10.1016/0022-2496(77)90033-5.